博士学位論文

# Studies on the multisensory integration in cricket's auditory system

（コオロギ聴覚系における多感覚統合に関する研究）

Makoto Someya

染谷　真琴

北海道大学大学院生命科学院

平成 30 年 9 月

学位論文内容の要旨

博士の専攻分野の名称　博士（生命科学）　氏名　染谷　真琴

学位論文題名

Studies on the multisensory integration in cricket's auditory system

（コオロギ聴覚系における多感覚統合に関する研究）

動物は異なる感覚器官で受容された複数のモダリティの感覚刺激の情報を中枢神経系で統合する。この過程は多感覚統合と呼ばれ，それによる神経活動の変化は物体の知覚や刺激によって誘導される行動の修飾をもたらす。多感覚統合は捕食者の検出感度の向上や，より正確な位置や距離の把握に有効であり，生存のための回避行動にも利益をもたらすと推測される。昆虫の中枢神経系には捕食者の接近に関連した刺激を検出するいくつかのニューロンが同定されているが，これらのニューロンが複数モダリティの感覚入力を統合しうるのかは不明であった。本学位論文では，捕食者であるコウモリが発する超音波エコーに応答するコオロギの聴覚ニューロン AN2 を対象として，やはり捕食者の接近を検知する気流感覚器である尾葉からの機械感覚入力と前肢鼓膜器官からの聴覚入力の多感覚統合に着目し，この問題に取り組んだ。

第一章では，AN2 を含む聴覚ニューロンが尾葉からの機械感覚入力を受けるかを検証した。尾葉は空気流の変化によって捕食者の接近を検出し，コオロギに逃避行動を引き起こす。まず，頸部腹側縦連合からの細胞外記録により，音刺激および気流刺激に応答する上行性神経活動を検証し，次に細胞内記録法により前胸神経節内における多感覚ニューロンを探索した。その結果，すでに聴覚ニューロンとして同定されている AN2, ON1 を含むいくつかの前胸介在ニューロンが気流刺激に対してスパイク応答を示した。気流応答は尾葉を切除すると消失したことから，鼓膜器官で受容された聴覚入力と尾葉で受容された気流感覚入力が，前胸神経節内の感覚情報処理の初期段階において統合されることが示唆された。

第二章では，聴覚および気流感覚入力が AN2 のスパイク発火に与える影響を検証した。音と気流刺激の同時提示刺激に対する応答はそれぞれの刺激の単独

提示に対する応答より有意に大きく，多感覚統合によって応答が増大されることがわかった。しかし，同時提示に対する応答は，基本的に単独提示に対する応答の和にほぼ等しく，AN2 は音と気流入力を線形に加算していた。単独提示応答の線形和よりも大きな加算は，スパイク閾値に近い弱い強度の刺激を同時提示した場合にのみ観察された。したがって，AN2 の多感覚統合における非線形加算は，興奮性シナプス後電位（EPSP）からスパイクへ変換する閾値特性を反映したものであると考えられる。

AN2 は音源の位置，音圧および音の長さといった情報を高頻度のスパイク発火(バースト発火)で符号化することが報告されている。音と気流の同時提示は，単独提示よりも高い頻度でバースト発火を誘発したことから，多感覚統合は音情報表現へも影響することが示唆された。しかし，単独提示した音刺激の強度を増大した場合にも同様にバースト発火は増大し，同程度の大きさのスパイク活動に含まれるバースト数は単独提示と同時提示に違いは見られなかった。したがって，バースト発火の増加は単にスパイク応答の増大によるもので，多感覚統合特異的なものではないと考えられる。したがって，AN2 は刺激のモダリティによらず興奮性入力を統合しており，その統合過程は一般的なシナプス入力加算のメカニズムによるものであると推測された。

第三章では，AN2 におけるバースト発火をもたらす神経基盤を理解する手がかりとして，感覚刺激のモダリティ，およびバースト発火と閾値以下の膜電位応答の関連を検証した。細胞内記録した AN2 の膜電位応答からスパイク成分を取り除き，閾値下の興奮性シナプス後電位（EPSP）を推定した。第二章においてほとんどのバースト発火は一発目の活動電位に続いて生じていたため， この初発スパイク後の EPSP に注目したところ，同時提示刺激に対する応答は単独提示刺激に対する応答よりも脱分極がより持続していた。この期間の脱分極の高とその持続時間は，いずれもバースト発火の発生および個々のバースト発火の大きさと相関を示したが，その関係性に刺激モダリティによる違いはみられなかった。以上の結果から，閾値以下の膜電位変化はバーストの発生およびその大きさを決定する重要な要因であるが，それに対する影響は入力強度の増大によるものであり多感覚統合特異的ではないことがわかった。

AN2 はコオロギの捕食者であるコウモリが発する超音波を検出し，そのバー

スト発火は飛行中のコオロギに音源と反対方向に飛行する逃避行動を引き起こすことから，捕食者検出ニューロンとして働くと考えられている。本研究によって，AN2 が尾葉への気流刺激に対しても興奮性の応答を示し，鼓膜からの聴覚入力と線形に加算したスパイク出力をすることによってバースト発生を増大させることがわかった。本研究結果は，感覚情報処理の初期に単一ニューロン内で複数のモダリティの感覚入力が統合され，逃避行動に利用されている可能性を示すものである。

# Contents

## General Introduction

The central nervous systems of animals integrate various modalities of signals detected by distinct sensory organs in a process known as multisensory integration (Pouget et al., 2002; Fetsch et al., 2013). Multisensory integration modulates the neural activity, which leads to improvement of sensory perception and enhancement of the behavioral responses to cross-modal stimuli compared to those of unimodal stimuli (Stein et al., 1988; Alais and Burr, 2004; Gu et al., 2008; McMeniman et al., 2014). For example, Human accurately perceives an object by integrating the visual and tactile signals (Ernst and Banks, 2002).

Thus, multisensory integration offers some advantages in detection of predators and in successful escaping because the attack of predator gives rise to multiple sensory cues. Several sensory interneurons in insects have been identified as detectors of predators' signals, and their activity elicits avoidance behaviors. For example, the visual interneurons, such as LPLC2 in fruit flies and DCMD in locusts are sensitive to looming motion stimuli that are perceived as an approaching predator. If the spiking responses of these neurons exceed a certain threshold, escape behavior is triggered (Fotowat and Gabbiani, 2007; Herberholz and Marquart, 2012; Klapoetke et al., 2017). The several identified auditory interneurons in crickets, moths, and mantids are also sensitive to ultrasound, such as the echolocation call of bats that prey on these insects, and activity of these neurons evoked by these stimuli elicits

defensive steering in flight (Hoy et al., 1989; Pollack, 2015). However, it remains unknown whether these key neurons are sensitive to multiple sensory cues relevant to a predator's attack. If these neurons have multimodal sensitivity, how are their spiking outputs altered by simultaneous sensory inputs of different modalities? To address these questions, which are main concerns of my dissertation, I testes multimodal sensitivity in prothoracic auditory neurons in the crickets, and focused on the auditory neuron 2 (AN2) that was identified as one of the multimodal neurons sensitive to both ultrasound and airflow.

# Chapter I

# Identification of Multimodal Neurons of Crickets

## 1.1 Introduction

Crickets process information on aero dynamics with two distinct sensory systems, cercal and auditory systems, which have the distinctly different sensory organs and frequency ranges of aero dynamics (Fig. 1-1A). Both sensory systems provide crucial signals of the predator attack and trigger the escape behavior.

The cerci are abdominal appendages covered with 500-750 filiform hairs that sense surrounding air particle displacement (Palka and Olberg, 1977; Miller et al., 2011). Information about airflow dynamics is processed by a local circuit within the terminal abdominal ganglion and transmitted by several ascending giant interneurons (GIs) (Fig. 1-1B) (Miller et al., 1991; Theunissen and Miller, 1991). The airflow signals detected by cerci are considered to be perceived as a sign of a predator's attack for crickets standing on the ground, because short air puff stimuli elicit running or jumping escapes (Tauber and Camhi, 1995; Oe and Ogawa, 2013; Sato et al., 2017).

On the other hand, sound with the higher frequency than 3 kHz (Imaizumi and Pollack, 1999) is detected by auditory receptor neurons of tympanal organ located at tibia of the front legs. The auditory receptor neurons project their afferent axons into the prothoracic ganglion (Hennig, 1988; Imaizumi and Pollack, 1999, 2005). Several prothoracic neurons directly receive excitatory synaptic inputs from auditory receptor afferents (Hennig, 1988). Sound information is conveyed by several kinds of ascending

projection neurons to brain (Hennig, 1988). The acoustic signals mediated by the ascending auditory neurons elicit escape steering during the flight (Nolen and Hoy, 1984; Schildberger and Hörner, 1988; Hedwig, 2006; Marsat and Pollack, 2012).

The cercal GIs project large long axon to brain and have axon collaterals arborizing into each segmental ganglion including the prothoracic ganglion (Hirota et al., 1993), suggesting the possibility that prothoracic auditory neurons are also sensitive to the airflow via the cercal system. Acually, it has been revealed that some prothoracic auditory neurons respond to wind stimuli (Atkins and Pollack, 1987). However, the wind sensitivity of auditory neurons related to avoidance behaviors has not been tested.

In this chapter, I explored whether the auditory neurons, which play key roles in the sensory coding relevant to biologically important events, receive the airflow inputs from cerci without the neural pathways through protocerebrum.

## 1.2 Materials and Methods

*Animals*

Adult female crickets (*Gryllus bimaculatus*) were used for the experiments. The crickets were bred and housed on a 12-h light/dark cycle at a constant temperature of 28°C.

*Extracellular recording*

For preparation of the extracellular recording, crickets were pinned dorsal side up on a silicone platform after removing the middle and hind legs. The connective nerve cords between the prothoracic and subesophageal ganglia were exposed by removing the gut and surrounding fat and were surgically cut to block the descending signals from the cephalic ganglia. Ascending spikes were extracellularly recorded using glass suction electrodes filled with isotonic saline placed proximally on the cut end of the nerve cord (Fig. 1-1A). For recording all ascending signals as multiple spike units, the whole nerve cord was suctioned by a glass micro-pipettes, while a part of ascending activities was recorded from a piece of split nerve cord for the single-unit recording. Signals were digitized at 20 kHz with a Powerlab 4/30 analog-digital converter (ADInstruments) and filtered with a 150–3,000 Hz band pass implemented in Chart version 7 software (ADInstruments).

Recorded spikes were sorted using a commercially available software (Spike Taro, Chinou Jouhou Shisutemu), which uses a sorting algorithm

based on the following two criteria: peak detection to separate individual units from a compound spike, and classification based on the correlation between separated units in terms of spike waveform and height. This algorithm has been used to analyze extracellular recordings of insect receptors (Kidokoro-Kobayashi et al., 2012). Spikes with heights in the range of ± 35% and waveforms with a correlation coefficient of >0.90 were considered to be generated by a single neuron. Units that fired more than once on average in a trial were selected for analysis. In the extracellular recording of the whole nerve cord, 134 units were sorted from 4 recordings.

*Stimulation for extracellular recording experiments*

The airflow stimulus consisted of short puffs of nitrogen gas from a nozzle connected to a PV820 pneumatic picopump (World Precision Instruments, Sarasota, FL, USA). Eight nozzles were arranged around the cerci on the same horizontal plane with their ends positioned 45° apart at a distance of 40 mm from the cerci. The velocity of airflow was 1.12 m/s as measured at the cerci. The duration of the airflow stimulus was 200 ms.

For sound stimulation, a 10-kHz pure tone was generated by RPvdsEx software (Tacker Davis Technologies, Alachua, FL, USA) and presented through 1.5 inch full-range sealed loudspeaker (MM-SPS2, Sanwa Supply, Okayama, Japan). Eight speakers were arranged around the cerci on the same horizontal plane with their ends positioned 45° apart. The duration of

115 sound pulses was 200 ms with symmetrical rise and fall times of 2 ms. The
116 sound intensity was 70 dB SPL in the recording from whole nerve cord and
117 76 dB SPL in the recording from a split nerve cord.

118 Single airflow or sound stimulus was provided independently from
119 various directions for multi-unit recording or from ipsilateral side to the nerve
120 cord for single-unit recording. To confirm whether the airflow was not
121 detected by the tympanum, responses to airflow and sound stimuli were
122 collected again after both frontal legs were ablated or both tympanums were
123 gummed up by adhesion bond.

124

125 *Intracellular recording*

126 For preparation of the intracellular recording, the wings and hind legs were
127 removed and the crickets were positioned ventral side-up on a block of clay
128 and restrained with small metal clamps. The prothoracic ganglion was
129 exposed and stabilized on a stainless-steel platform using a silver wire ring.
130 To eliminate descending signals from the cephalic ganglion, the connective
131 nerve cords between the prothoracic and subesophageal ganglia were cut. In
132 the ablation experiment, both cerci were removed to confirm that the auditory
133 neurons received the sensory signals from the cerci.

134 Glass microelectrodes (40-60 MΩ) were filled with 8% Lucifer yellow CH
135 lithium salt (Sigma-Aldrich, RRID:SCR_008988) in 200-mM LiCl or 2-mM
136 Oregon Green BAPTA-1 hexapotassium salt in 200-mM potassium acetate.

137 Lucifer yellow was used for most of the recordings and both kinds of the
138 electrode solution have no influence on the spontaneous activities and neural
139 responses. Glass microelectrode was inserted into dendrites or axons of
140 auditory neurons and membrane potentials of recorded neurons were
141 measured with current clamp mode. Electrophysiological signals were
142 digitized at 20 kHz with a Powerlab 4S analog-to-digital converter
143 (ADInstruments) and recorded with Chart version 7 software
144 (ADInstruments). To load the fluorescent dye, a hyperpolarizing current of −1
145 to −2 nA was injected during recording. To identify the recorded neuron, the
146 prothoracic ganglion was dissected after recording, fixed in 4%
147 paraformaldehyde in 200-mM phosphate buffer over night, dehydrated for 15
148 min each in a series of 50, 70, 90, 100, and 100% ethanol, and cleared in
149 methyl-salicylate.
150
151 *Stimulation in the intracellular recordings*
152 The airflow stimulus consisted of short puffs of nitrogen gas from a nozzle
153 connected to an IM-300 microinjector (Narishige, Japan). For stimulation, the
154 nozzle ends were positioned 15 mm away from the cerci on either side of the
155 cricket. The duration of the airflow stimulus was 200 ms. The velocity of
156 airflow was from 0.17 to 0.43 m/s (see each figure legend). For finding the
157 auditory neurons, 5- or 15-kHz pure tone was generated by RPvdsEx software

158 (Tacker Davis Technologies) and presented through an ATH-CM707
159 headphone speaker (audio-technica, Tokyo, Japan). A pair of speakers were
160 positioned 25 mm away from the tympanum on either side. The duration of
161 sound pulses was 30 ms with symmetrical rise and fall times of 2 ms. The
162 sound intensity was 60 dB SPL.
163
164 *Data analysis*
165 Spike traces were binned at 20-ms resolution through all figures in this
166 chapter. To analyze subthreshold voltage traces, raw traces of the recordings
167 were filtered by a median filter with a 5-ms window (Shi et al., 2017). Then,
168 the resting level of membrane potential was subtracted from the filtered
169 potentials to indicate the stimulus-evoked postsynaptic potentials. The
170 latency of EPSP was defined as the duration from the stimulus onset to the
171 points when the filtered potential exceeded 3 mV, which corresponded to 2 SD
172 (2.89 mV) of the spontaneous fluctuation in the resting potentials of AN2 and
173 omega neuron 1, from the resting potential.
174 MATLAB software (MathWorks, RRID:SCR_001622) was used for data
175 processing and analysis, and R programming software v3.4.0 (R Core Team
176 2013) was used for statistical analysis. To avoid pseudoreplication, the data
177 obtained from the same samples were averaged for each individual. All values
178 are reported as mean ± standard error of the mean. A $p$-value of $< 0.05$ was
179 considered to be statistically significant.

## 1.3 Results

### 1.3.1 Exploring multimodal neurons by extracellular recordings

First, I examined existence of ascending multimodal neurons in the thoracic or abdominal ganglia that responded to the acoustic and airflow stimuli. The spiking responses of the ascending neurons to the sound stimulus applied to tympanums and the airflow stimuli applied to cerci were extracellularly recorded from the distal cut end of a nerve cord between the subesophageal and prothoracic ganglia (Fig. 1-2A, B). Individual spikes were sorted into multiple units based on their wave shapes of spikes (see Methods). I found multi-modal units which showed firing responses to both sound and airflow stimuli (Fig. 1-3A, B). These multimodal units accounted for 46% of all sorted units (Fig. 1-3C). Thirty percent of units were sensitive to only airflow stimuli, but no units responded to only sound stimuli. The multimodal units showed remarkable increase in spiking activity in responses to the both stimuli (Fig. 1-3D). The auditory responses completely disappeared after the tympanums were removed (Fig. 1-3D). After the tympanum removal, 96% of them showed no significant increase in spiking responses to sound (unpaired t-test). These results indicate that a part of ascending neurons is sensitive to both airflow and sound stimuli.

However, the multi-modal units might contain multiple cellular activities derived from auditory-specific and cercal-specific neurons or activity of a single cell might split into multiple units. To confirm the

existence of multimodal neurons, single unit recording was performed from a split nerve cord (Fig. 1-4A). In the single unit recording, the multimodal spike unit was recorded, which showed spiking responses to both sound and airflow stimuli (Left 2 panels in Fig. 1-4B, C). After both tympanums were covered with adhesion bond, the units showed no response to the sound while it still responded to the airflow. This result also supported the existence of ascending multimodal neurons in the thoracic or abdominal ganglia.

### 1.3.2 Multimodal neurons in the prothoracic ganglion

To identify the multimodal neurons observed with extracellular recordings, I performed intracellular recording in the prothoracic ganglion to monitor the membrane potential responses to auditory and airflow stimuli and to stain the recorded neuron with fluorescent dye. I found that ascending neuron identified as AN2 and local interneuron identified as omega neuron 1 (ON1), both of which have been identified as the auditory ascending neuron (Wohlers and Huber, 1982), were sensitive to the airflow stimuli to cerci (Fig. 1-5A, B). Their responses to the airflow were significantly larger in the firing rate than the spontaneous activities (Fig. 1-5C). In addition to AN2 and ON1, omega neurons 2 (ON2), T-shape neuron 1 (TN1) and descending neuron 1 (DN1) also showed distinct spiking responses to airflow stimuli. However, their airflow-evoked responses were no significance statistically because of small size of samples. In contrast, the auditory ascending neuron 1 (AN1) showed

no response to the airflow stimuli (Fig. 1-6A, B), of which firing rate and membrane potential during the airflow stimulation were not different from their spontaneous activity (Fig. 1-6C, D). My results demonstrated that certain types of auditory neurons including ascending, descending, and local interneurons have bi-modal sensitivity.

### 1.3.3 Response property of the auditory neurons to airflow stimulation

Next, I examined the response properties of AN2 and ON1 to airflow stimuli (Fig. 1-7A). In both AN2 and ON1, the airflow stimulus evoked transient firing (Fig. 1-7B). The latency from stimulus onset to the first spike in AN2 was shorter than that in ON1 although this time difference was not significant (Fig. 1-7C). I observed no difference in their firing rate in the transient spiking responses (Fig. 1-7D) and during the later phase following the transient response (Fig. 1-7E).

There was significant difference in the time course of the subthreshold membrane potential changes between AN2 and ON1 (Fig. 1-8A). Both AN2 and ON1 showed transient depolarization of their membrane potential in response to airflow stimuli. In AN2, the depolarized membrane potential quickly returned to the resting level. In contrast, ON1's membrane potential depolarization was sustained even after the stimulus termination. The latency of EPSP of AN2 was shorter than that of ON1 (Fig. 1-8B). There was no difference in EPSP amplitude during the transient phase (Fig. 1-8C),

246 whereas the EPSP during the later phase following the transient
247 depolarization was larger in ON1 than AN2 (Fig. 1-8D). Therefore, although
248 both AN2 and ON1 show transient depolarization in response to airflow
249 stimuli, ON1's EPSP was longer lasting and evoked sustained firing. This
250 difference in time course of the responses suggests that different neural
251 pathways convey the airflow signals to the ascending and local interneurons.
252 ON1 shows directional selectivity for the auditory stimulus and plays a
253 prominent role in producing the directionality of AN1 and AN2 (Selverston et
254 al., 1985; Horseman and Huber, 1994). Thus, I investigated the directional
255 selectivity for airflow stimulus in ON1. ON1 tended to generate more spikes
256 in response to the airflow stimuli from ipsilateral to its soma than to the
257 contralateral stimuli (Fig. 1-9A, B). There was no difference in the latency
258 from stimulus onset to the first spike between the stimulus directions (Fig. 1-
259 9C). Since ON1 prefers the ipsilateral stimulus to its soma in its auditory
260 response (Wohlers and Huber, 1978), the directional preference in the airflow
261 response coincided with that for auditory stimuli.
262 Finally, I examined whether the cercal system mediated the airflow-evoked
263 excitatory synaptic inputs to AN2 and ON1. As shown in Fig. 1-7A and 1-8A,
264 AN2 and ON1 showed remarkable EPSPs and spiking responses to airflow
265 stimuli. In the individuals of which both cerci were ablated, both AN2 and
266 ON1 showed no change in their membrane potential in response to the airflow
267 stimuli (Fig. 1-10), meaning that the mechanosensory signals to AN2 and

268 ON1 are mediated by the cercal system.

## 1.4 Discussion

In this study, I demonstrated that certain types of prothoracic auditory neurons including AN2 were sensitive to mechanosensory stimuli received via the cercal organ. On the other hand, AN1 considered to be a key neuron to elicit positive phonotaxis (Schildberger and Hörner, 1988) was insensitive to the airflow. AN1 responds to calling songs of male crickets, of which carrier frequency is about 5 kHz (Horseman and Huber, 1994), and induces oriented walking behavior in female attracted by the male's song (Schildberger and Hörner, 1988). In contrast, AN2 responds to ultrasound like echolocation call of bats that prey on the crickets. Thus, our results suggest that the airflow signals would influence the processing of auditory information relevant not to mating but to predators. Further, I revealed that ON1 was also sensitive to mechanosensory stimuli. This local interneuron inhibits activities of the contralateral ON1, AN1 and AN2, resulting in the enhancement of the directional selectivity in AN1 and AN2 (Selverston et al., 1985; Horseman and Huber, 1994). The airflow-driven activity of ON1 might modulate the directional selectivity of AN1 and AN2.

The interneurons AN2, ON1, ON2, TN1 and DN1, which were examined in this study, have been identified as auditory neurons in the prothoracic ganglion (Wohlers and Huber, 1982). Some previous studies have reported that these auditory interneurons are also affected by other modalities of sensory inputs. For example, AN2 and ON1 receive inhibitory inputs from

291 mechanoreceptors within the subgenual organ of legs which detects
292 mechanical vibration (Wiese, 1981; Kühne et al., 1984). TN1 and DN1
293 responds to wind stimuli (Atkins and Pollack, 1987). In addition to these
294 interneurons, certain T-shaped neurons, which extend both ascending and
295 descending axons, and descending neurons are sensitive to sound, wind and
296 light stimuli (Atkins and Pollack, 1987). These findings indicate that the
297 auditory information is not processed by modality-specific pathways. Rather,
298 the sensory systems within the prothoracic ganglion process multiple sensory
299 modalities. Notably, AN2 directly receive excitatory inputs from receptor
300 neurons in the tympanum (Hennig, 1988). Considering this previous finding
301 and my results together, inputs from multiple sensory modalities are
302 integrated in the early stage of sensory processing.

303 I demonstrated that the airflow inputs to AN2 and ON1 was mediated
304 by the cercal system. Neural pathways from the cerci to wind sensitive
305 auditory interneurons remain unclear. However, the wind-sensitive giant
306 interneurons (GIs), which project their ascending axons to the brain, arborize
307 their axon-collaterals into the thoracic ganglion (Hirota et al., 1993). Most of
308 the GIs show directional selectivity and prefer airflow from ipsilateral side to
309 their axons (Jacobs et al., 2008). ON1 also had directional preference for the
310 airflow from ipsilateral side to its soma, which suggests that GIs with their
311 axons ipsilateral to ON1's cell body provide airflow inputs to ON1.

312 Fig. 1-1.

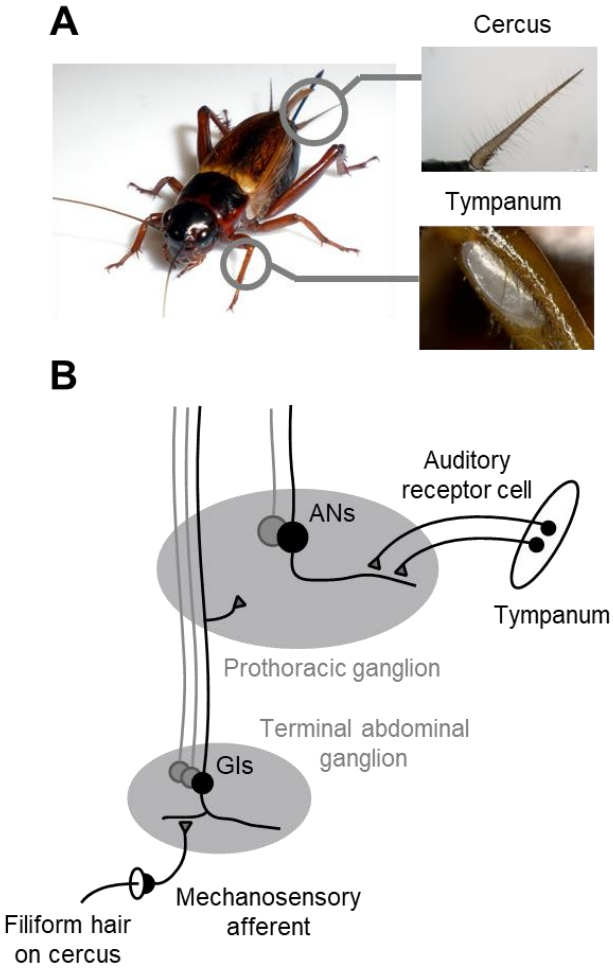
A
Cercus
Tympanum
B
Auditory
receptor cell
ANs
Tympanum
Prothoracic ganglion
Terminal abdominal
ganglion
GIs
Mechanosensory
afferent
Filiform hair
on cercus

Figure 1-1. Auditory and cercal sensory systems of crickets. A) Two sensory organs, tympanum and cercus. B) Diagram indicating the auditory and cercal-sensory pathways. GIs, wind-sensitive giant interneurons; ANs, auditory ascending neurons.

317 Figure 1-2

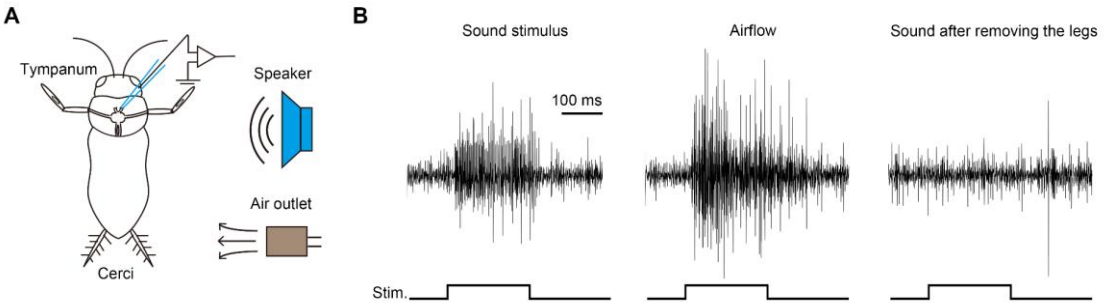


318

Figure 1-2. Extracellular recordings of ascending neurons. A) Experimental setup for extracellular recording and stimulation. B) Typical ascending activities evoked by sound (left panel) and airflow (middle). Right panel shows sound-evoked response after both frontal legs were removed. Lower rectangular traces indicate the stimulation.

324 Figure 1-3

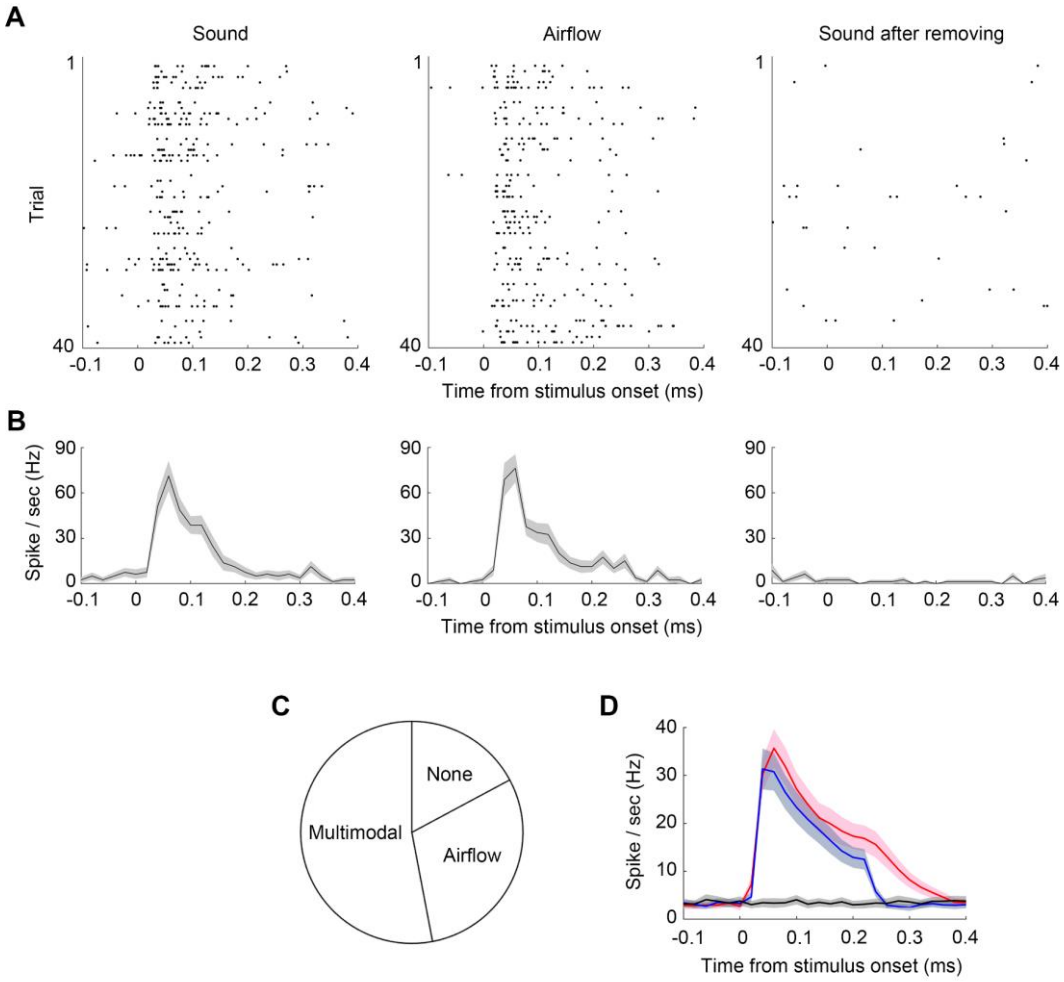


325

Figure 1-3. Ascending spike units responding to airflow and sound stimuli. A) Raster plot of a typical multimodal unit sensitive to sound and airflow. Each dot indicates individual spike for sound (left), airflow (middle) and sound stimulations after the frontal legs were removed (right). B) Time course of firing rates of the unit shown in A. Stimulation in each column corresponds to that in Fig. 1-3A. C) Fraction of multimodal, airflow-specific, and non-responsive spike units in all recorded units. Each unit was labeled whether its firing rate during the stimulation was significantly different from spontaneous firing rate (paired t-test and Holm-Bonferroni correction). D) Time course of mean firing rate of all multimodal units for sound (blue), airflow (red), and sound stimulation after leg removal (black).

337 Figure 1-4

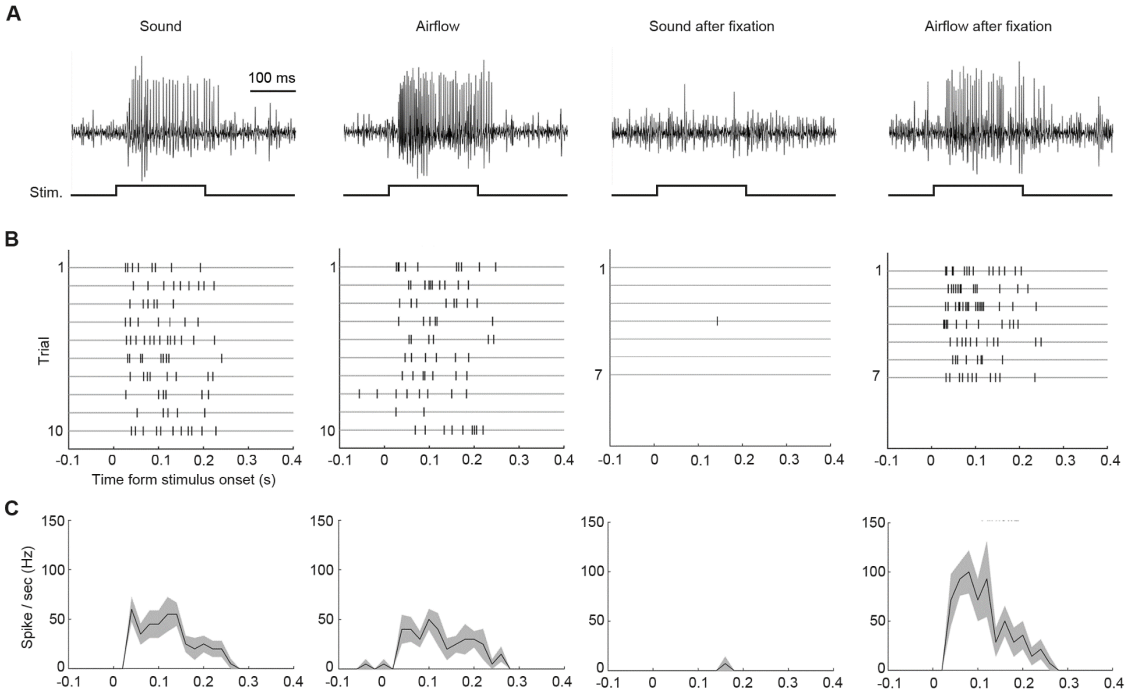


338

Figure 1-4. Single-unit recording of ascending neurons from the split nerve cord. A) Raw traces of typical ascending activities for sound and airflow stimulations in naïve (left two panels) and auditory-blocked (right two panels) crickets in which both tympanums were gummed up. B), C) Raster plots (B) and time course of the firing rate (C) of typical multimodal unit shown in Fig. 1-4B. Stimulation for each column corresponds to that in Fig. 1-4A.

345 Figure 1-5

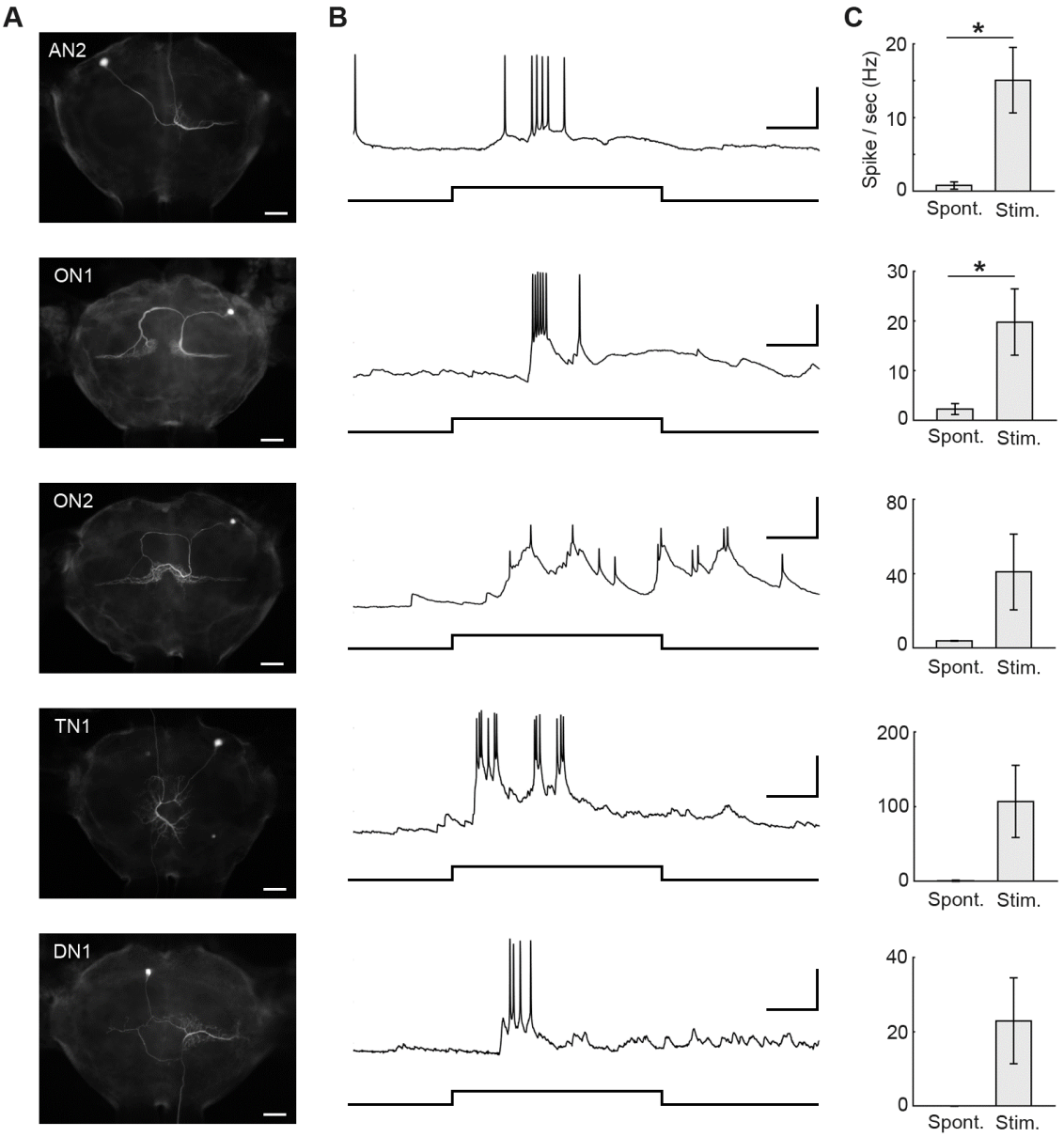

Figure 1-5. Airflow-evoked membrane-potential responses in identified auditory neurons. A) Fluorescent images of auditory neuron AN2, ON1, ON2, TN1 and DN1 recorded intracellularly. Scale bars indicate 100 µm. B) Typical traces of membrane potential during the airflow stimulation. Lower rectangular traces indicate the airflow stimulation. Vertical and horizontal scale bars indicate 20 mV and 50 ms, respectively. C) Mean firing rate during the spontaneous activity (Spont) and airflow stimulation (Stim), each of which was measured as mean value for 200 ms before or during the airflow stimulation. Sample sizes were 11 AN2s, 8 ON1s, 2 ON2s, 3 TN1s and 3 DN1s (paired t-test, $p_{AN2} = 0.06 \times 10^{-1}$, $p_{ON1} = 0.04$, $p_{TN1} = 0.16$ and $p_{DN1} = 0.18$). The cell type in each row corresponds to that in Figure 1-5A. Velocity of airflow stimulus was from 0.17 to 0.43 m/s.

358 Figure 1-6

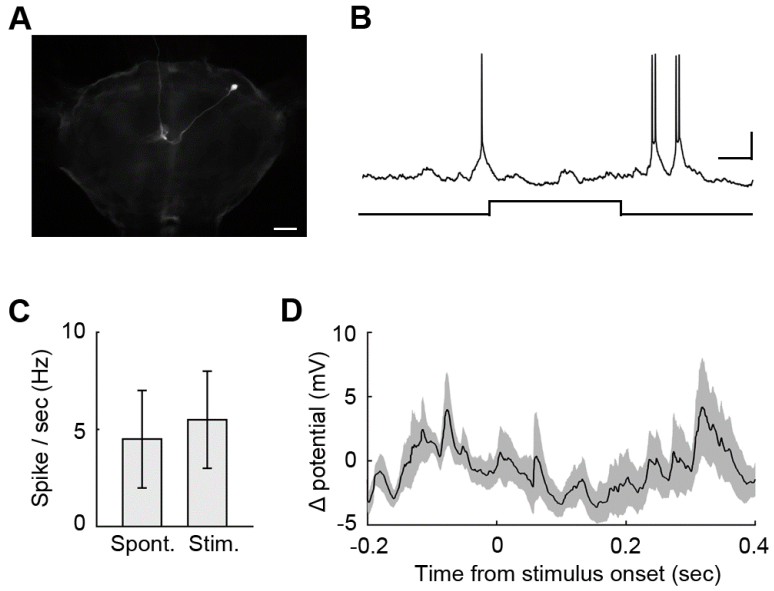


359

Figure 1-6. Neural response of AN1 to airflow stimulus. A) Fluorescent image of AN1. Scale bar indicates 100 μm. B) Typical trace of membrane potential in AN1 for airflow stimulation. Vertical and horizontal scale bars indicate 10 mV and 50 ms, respectively. C) Firing rate during spontaneous activity (Spont) and stimulation (Stim) (n = 2 AN1s). D) Subthreshold change in the membrane potential in AN1. After action potentials were removed using a median filter with 5-ms window, the difference in the filtered membrane potential from the average of resting potentials before stimulation was calculated. Velocity of airflow stimulus was 0.43 m/s, and stimuli were delivered from contralateral side to AN1's soma.

370 Figure 1-7

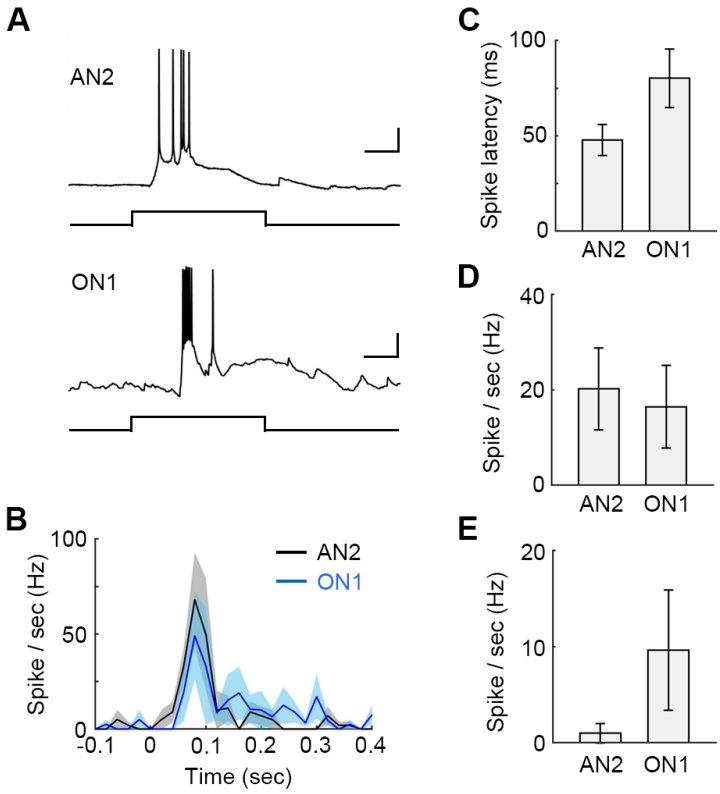

Figure 1-7. Firing-response properties of AN2 and ON1 for airflow stimulation. A) Typical traces of membrane potentials in AN2 and ON1. Vertical and horizontal scale bars indicate 10 mV and 50 ms, respectively. B) Time course of firing rate in AN2 and ON1 (n = 5 neurons respectively through Fig. 1-7). C) Latency from stimulus onset to the evoked first spike (Wilcoxon rank sum test, $p = 0.10$). D) Firing rates in the earlier phase within 200 ms after the stimulus onset (unpaired t-test, $p = 0.77$). E) Firing rates in the later phase which was time period from 200 to 300 ms after the stimulus onset (unpaired t-test, $p = 0.24$). Velocity of airflow stimulus was 0.18 m/s. Stimuli were delivered from ipsilateral side to ON1's soma and from contralateral side to AN2's soma.

382 Figure 1-8

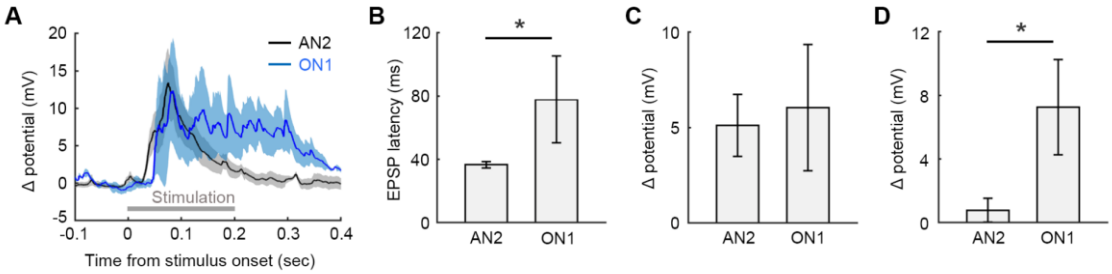


383

Figure 1-8. Subthreshold membrane-potential response properties of AN2 and ON1 for airflow stimulation. A) Time courses of subthreshold activity in AN2 (black; n = 5 neurons) and ON1 (blue; n = 3 neurons). Gray line indicates the airflow stimulation. B) Latency of EPSPs evoked by airflow stimulus (sample size was the same as shown in A through B-D; Wilcoxon rank sum test, $p = 0.04$). C) Mean postsynaptic potentials in the earlier phase within 200 ms after the stimulus onset (unpaired t-test, $p = 0.78$). D) Mean potentials in the later phase which was time period from 200 to 300 ms after the stimulus onset (unpaired t-test, $p = 0.04$). Velocity and direction of stimulus are the same as shown in Fig. 1-7.

394 Figure 1-9

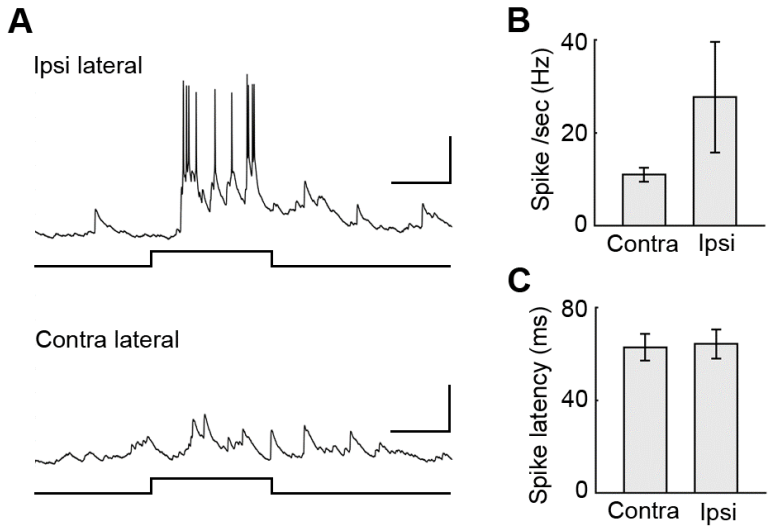

Figure 1-9. Directional selectivity to airflow stimulation in ON1. A) Typical traces of membrane potentials in ON1 during airflow stimuli from ipsil- (upper) or contralateral (lower) side to its soma. B) Mean firing rates in responses to ipsil- (Ipsi) or contralateral (Contra) stimulation (n = 3 neurons; paired t-test, $p = 0.29$). C) Latency from the stimulus onset to the first spike for ipsil- or contralateral stimulation (n = 3 neurons; Wilcoxon signed-rank test, $p = 0.75$). Velocity of airflow stimulus was 0.18 m/s.

405 Figure 1-10

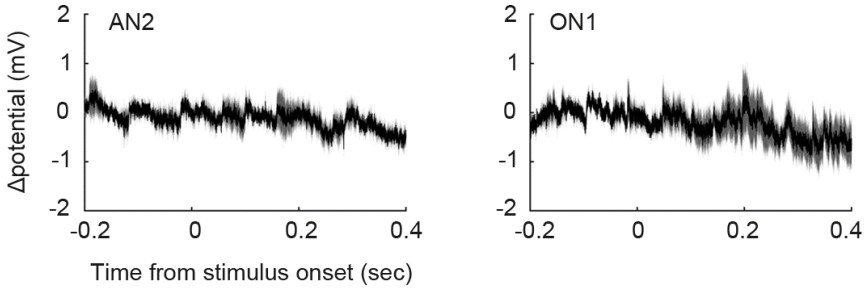


406

Figure 1-10. Airflow-evoked responses in AN2 and ON1 without cerci. Time courses of difference in the raw membrane potentials in AN2 and ON1 for airflow stimulation after the both cerci were ablated. Velocity of airflow stimulus was 0.17 m/s.

# Chapter Ⅱ

# Multisensory Integration in an Auditory Neuron AN2

## 2.1 Introduction

In the previous chapter, I demonstrated that AN2 was sensitive to airflow stimuli to cerci. AN2 is one of the primary auditory interneurons that receives direct synaptic inputs within the prothoracic ganglion from auditory receptor neurons of the tympanal organ located in the tibia of the front legs (Wohlers and Huber, 1982; Hennig, 1988). This neuron is sensitive to high-frequency sounds (Wohlers and Huber, 1978; Popov and Markovich, 1982), and its high-frequency firing responses can trigger an avoidance steering response in flying crickets (Nolen and Hoy, 1986). Therefore, AN2 is considered to be a neuron that detects the presence of bats. The location of the sound source and its intensity and duration are encoded by 'burst firing' of AN2 with short inter-spike intervals, the behavioral functions of which have been well studied (Marsat and Pollack, 2005, 2006, 2010). My previous finding of the airflow-sensitivity of AN2 suggests that AN2 could detects other modality of sensory clue of a bat's attack, such as strong turbulent airflow caused by the bat's wingbeats.

It has been reported that the simultaneous presentation of different modal stimuli, termed as cross-modal stimulation, elicits enhancement or depression of spiking responses comparing to those responses to each component stimulus (Meredith and Stein, 1983). Furthermore, enhancement in cross-modal stimulation results in nonlinear (supra- or sub-linear) or linear summation of unimodal responses (Stein and Stanford, 2008). In this chapter,

I examined multisensory integration in the spiking outputs of AN2 in response to the cross-modal stimulus combining the sound and airflow.

In addition, cluster of spikes in short intervals, called bursts, plays an important role in the sensory signaling by AN2. The burst firing of AN2 can improve the detection of sound stimuli and the representation of sound-source location (Marsat and Pollack, 2006). The fine temporal structure of the burst firing represents additional stimulus-related information such as intensity and duration of sound (Marsat and Pollack, 2010). Thus, I also examined effect of the multisensory integration on burst firings in AN2.

## 2.2 Materials and Methods

See the method in Chapter I about *Animals* and *Intracellular recordings*. Throughout the experiment in this chapter, 4 or 8% Lucifer yellow CH lithium salt in 200-mM LiCl was used for intracellular recordings.

*Stimulation*

See Methods in Chapter I about the apparatuses for airflow and sound stimulations. The velocity of airflow was 0.17 m/s at the position of cerci and the duration was 200 ms. For sound stimulation, only 15-kHz pure tone was used.

For unimodal stimulation of the cerci, single air puffs were used (Fig. 2-1). Different manners of stimulation were used for experiments with repetitive stimulation or various auditory intensities. In the repetitive-stimulation experiments that were performed to test multisensory integration, 9 sound pulses at 60 dB were given with 500-ms inter-stimulus interval, and airflow was provided coincident with the 4th sound pulse. To analyze multisensory effects, I compared the responses to the 3rd sound pulse with those to the combined stimuli. All responses to sound pulses (1st-3rd and 5th-9th) were used for comparing burst firing with non-burst firing. In the experiments with varying auditory intensities that were performed to test the effects of input amplitude, single sound pulses of 50, 60, 70, 80, or 90 dB were applied for the unimodal stimulation, and a single air puff combined with

various intensities of sound pulses was applied for the cross-modal stimulation. All stimuli were delivered contralateral to the soma of the recorded AN2. For the cross-modal stimuli with both types of stimulation, differences in the stimulus onset between the sound pulse and airflow were < 15 ms, and the onset of the sound stimulus was defined as the stimulus onset for cross-modal stimuli.

*Data analysis*

In the repetitive stimulation experiments, neural responses to sound pulses, airflow, and combined stimuli were recorded from 8 neurons in different crickets. In the various intensities experiments, the responses to sound pulses were recorded from 4 neurons in different crickets, and those to airflow and combined stimuli were obtained from 3 out of these 4 neurons. In addition to these experiments, responses to airflow stimuli were also recorded from 5 neurons. In the cerci ablation experiments, neural responses to airflow stimuli were recorded from 2 neurons in 2 crickets. Spikes were detected using custom-written MATLAB routines (R2016a, MathWorks, RRID:SCR_001622). Raw traces of membrane potential were filtered with a 150-Hz high-pass filter, and spike peaks were detected based on the filtered traces using the findpeaks function in MATLAB. To analyze the time course of the firing rate, spike trains were binned at a size of 1 ms and convolved with a moving-average filter with a 20-ms window. Summation of the

488 responses ($r_{sum}$) to the uni-modal stimulus was defined as

489 $$r_{sum} = r_{sound} + r_{airflow}$$

490 where $r_{sound}$ and $r_{airflow}$ indicate the firing rate in response to sound or
491 airflow stimulus, respectively. Linearity of the multisensory integration was
492 defined as

493 $$Linearity = \frac{r_{cross}}{r_{sum}}$$

494 where $r_{cross}$ indicates the firing rate in the response evoked by the cross-
495 modal stimulus. Histogram of inter-spike intervals (ISI) was fitted to a kernel
496 probability distribution using normal kernel smoothing with a 0.3-ms
497 bandwidth. To test the ISI distribution results from a Poisson process, the ISI
498 histogram was also fitted to a single exponential curve. A burst was defined
499 as a cluster of spikes separated by short intervals (< 6.5 ms; Marsat and
500 Pollack 2006). The first and last spike within a burst were defined as the
501 onset and offset of the burst, respectively. Size of the burst was defined as a
502 product of the burst duration and the number of spikes within the burst
503 (Marsat and Pollack, 2010).

## 2.3 Results

### 2.3.1 Multisensory enhancement in AN2 spiking activity

To examine the multisensory effects of simultaneous inputs with different modalities on the spiking activities of AN2, I compared neural responses to single air puffs, the 3rd sound pulses, and cross-modal stimulation combining an air puff with the 4th sound pulse (Fig. 2-2A). Cross-modal stimuli elicited significantly larger numbers of spikes than unimodal stimuli did, but the amplitudes of the responses to the cross-modal stimuli were similar to the arithmetic sum of the responses to the 3rd sound pulse and air puff that were separately presented (Fig. 2-2A, B). The linearity of the responses to cross-modal stimuli was examined using various intensities of sound combined with airflow, the velocity of which was constant (Fig. 2-2C). Higher intensities of sound stimuli elicited greater spiking responses in both uni- and bimodal stimulus conditions, but the responses to cross-modal stimuli were close to the arithmetic sum of the responses to airflow and to sound pulses regardless of the sound intensity. To verify the effects of the sound intensity on the linearity of the summation in the cross-modal responses, I examined the relationship between the linearity of summation and firing rates in the summed responses to unimodal stimuli (Fig. 2-2D). Linearity depended on the magnitude of the summed responses, and supra-linear summation was observed only in small responses in which the firing rate was lower than 10 Hz. This suggests that AN2 linearly and additively integrates auditory and

526 mechanosensory input, and supra-linear summation occurred in the
527 integration of small sensory inputs evoked by stimuli around the threshold.
528 The linearity of summation in the cross-modal responses could depend
529 on the stimulus intensity (Meredith and Stein, 1986; Stein and Stanford,
530 2008) but also on the latency from stimulus onset (Rowland and Stein, 2007;
531 Rowland et al., 2007). Thus, I examined the temporal profile of the
532 summation linearity. The cross-modal responses were larger in their firing
533 rate than sound-evoked responses (Fig. 2-3A) and the arithmetic sum of
534 unimodal responses (Fig. 2-3B) during the period of 30–60 ms after stimulus
535 onset. However, there was no significance in the firing rates in this period
536 between the cross-modal and summed responses (n = 8 neurons, paired t-test,
537 $p = 0.07$, the firing rates were $85.05 \pm 10.44$ Hz for cross-modal and $66.61 \pm$
538 13.00 Hz for the summed responses, respectively). In addition, even if I
539 focused on this period, the supra-linear summation occurred only in the small
540 cross-modal responses (Fig. 2-3C). The supra-linear summation would simply
541 result from the fact that summed inputs of the subthreshold unimodal stimuli
542 were larger than the spike threshold and evoked action potentials. Our
543 results suggest that AN2 linearly sums auditory and mechanosensory inputs
544 and that supra-linearity cross-modal summation would arise from the spike
545 threshold.
546
547 **2.3.2 Multisensory enhancement in burst firing of AN2**

548 In previous studies (Marsat and Pollack, 2006, 2007), the responses of AN2
549 to 30-kHz long-duration tones with Gaussian amplitude envelopes showed a
550 characteristic distribution of inter-spike intervals (ISI), with a peak at short
551 intervals and broad tail of longer intervals. Based on this ISI distribution, the
552 spike trains with intervals shorter than 6.5 ms are classified into 'bursts,'
553 which are used for encoding precise ultrasound information (Marsat and
554 Pollack 2006, 2010). In the current study, ISI distribution of the multiple
555 spikes that were evoked in 58% of responses (170/294 in 17 individuals) to 15-
556 kHz tone pulses at 60 dB showed similar features, which included a peak at
557 short intervals and a peaky but broad tail at longer intervals (Fig. 2-4A). In
558 addition, the bimodal peaks in ISI distribution in our data could be also
559 separated at 6.5 ms intervals. To confirm that the peak at the shorter
560 intervals indicated the distribution of the burst firing, I fitted a single
561 exponential curve to the whole ISI histogram. If the peaks surpass this curve,
562 these activities were considered to be burst firings different from the ISI
563 distribution expected by Poisson process (Bastian and Nguyenkim, 2001;
564 Marsat and Pollack, 2012). The distinct peak at the intervals shorter than 6.5
565 ms was higher than the exponential curve, indicating that the 15-kHz tone
566 pulse stimulus enabled AN2 to generate the burst firings, which could be
567 separated from the isolated spikes using the same criteria as in previous
568 studies.

569 I examined effects of cross-modal stimuli on generation of burst firing.

570 Burst firing responses were more frequently evoked by cross-modal stimuli
571 than by unimodal stimuli (Fig. 2-5A). To clarify whether this enhancement of
572 burst firing activity was specific to multisensory integration or simply
573 resulted from increased firing rates due to linear summation, I evaluated the
574 effects of response magnitude on the probability of burst occurrence among
575 cross- and unimodal responses. The larger the spiking responses were, the
576 higher the probability of burst occurrence was regardless of the sensory
577 modality (Fig. 2-5B). Further, there was little difference among the uni- and
578 cross-modal responses in the dynamic ranges of the curves, that indicated a
579 relationship between the response magnitude and the bursting probability.
580 This means that multisensory integration does not specifically affect the
581 generation of burst firing. Rather, more frequent burst firing would result
582 simply from an increase in spiking responses via linear summation of
583 auditory and mechanosensory inputs.

584 I also focused on temporal aspects of burst generation (Fig. 2-5C). Most
585 of the bursts occurred following the first action potentials evoked by the
586 auditory and cross-modal stimuli. In contrast, the bursts evoked by the
587 airflow stimuli followed several isolated spikes to appear in the middle of
588 spike trains. Taken together, these results illustrate that AN2 integrates
589 sound and airflow inputs and enhances the response magnitude, resulting in
590 burst firing activity at the beginning of responses. However, the bursts were
591 also enhanced by stronger unimodal stimuli, and no difference in the timing

592 of burst generation was observed between the auditory and cross-modal
593 responses.
594
595 **2.3.3 Effect of temporal coincidence of the stimuli on the burst firing**
596 In multisensory integration, the neural responses to the cross-modal
597 stimulus were enhanced when the stimuli were presented at the same time
598 and/or provided from the same location (Holmes and Spence, 2005). This
599 spatio-temporal coincidence detection is considered as a mechanism to
600 precisely detect a single event or object presenting multiple sensory cues. To
601 examine whether AN2 responses to the cross-modal stimulus depended on
602 the timing of stimulus presentation, the sound and airflow stimuli were
603 provided in various intervals between them (Fig. 2-6A). The number of spikes
604 evoked by stimulus did not depend on the temporal difference in the stimulus
605 onset (Fig. 2-6B). However, the cross-modal stimuli elicited a single burst
606 when the airflow and sound stimuli were presented at approximately the
607 same time (Fig. 2-6C). When the stimulus onsets separated over 40 ms, AN2
608 generated multiple bursts. To focus on the temporal structure of burst, I
609 measured the duration and size, which is product of number of spikes within
610 burst and duration of burst and is positively correlated with magnitude of the
611 behavioral response (Marsat and Pollack, 2010). Figures 2-6D and 2-6E show
612 the relationships between the time lag between sound and airflow stimuli and
613 the maximum duration or maximum size of the burst, both of which were

614 measured from the largest burst in the response if multiple bursts were
615 evoked. Both duration and size became larger as the difference of stimulus
616 interval was shorter (Fig. 2-6D, E). Not only the maximum duration and size
617 of the individual burst, but the summation of size in all bursts elicited by a
618 single stimulation also depended on the difference of stimulus onset (Fig. 2-
619 6F, G). These results suggest that AN2 represents the coincidence of the
620 stimulus onsets by using the temporal structure of burst.

## 2.4 Discussion

I demonstrated that the cross-modal stimulation enhanced the magnitude of firing activity. Further, simply put, the spike outputs evoked in AN2 by cross-modal stimuli were equal to linear summation of those evoked by the respective unimodal stimuli. Supra-linear summation in spiking activity was observed only when the unimodal stimuli were as weak as the threshold for generating spikes, suggesting that supra-linear summation would result from the non-linear transduction from graded potentials to action potentials by threshold properties of voltage-gated channels (Holmes and Spence, 2005). Our result that supra-linear summation was observed only around spike threshold is consistent with that in recent studies of the MSTd (dorsal medial superior temporal) area of macaques (Morgan et al. 2008) and the superior colliculus of cats (Perrault et al., 2003, 2005; Stanford, 2005). Because the supra-linearity of the spike threshold is based on intrinsic active membrane properties, the supra-linear summation of spike responses of AN2 would not be specific to multisensory integration.

As well as the mean firing rate of the response, the burst firing was also enhanced by the cross-modal stimulation. Considering that AN2 uses bursts to encode the sound information such as intensity, duration, and location (Marsat and Pollack, 2006, 2010), airflow stimulus would have some impacts on acoustic representation in AN2. Although it is unclear the role of cercal signals on the acoustic representation in AN2, multisensory integration may

643 improve neural representation of the component stimulus (Ibrahim et al.,
644 2016; Atilgan et al., 2018).

645 Figure 2-1

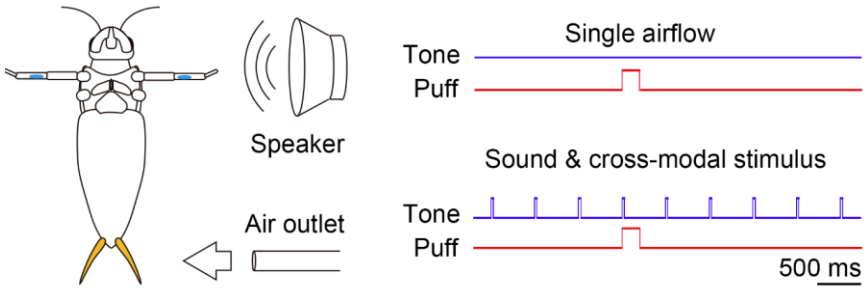

Figure 2-1. Experimental setup (left) and stimulation protocol of repetitive-stimulation experiments (right). Single short durations of airflow were delivered separately (upper). Nine tone pulses were repetitively applied and single airflow stimuli were combined with the 4th pulse (lower).

650 Figure 2-2

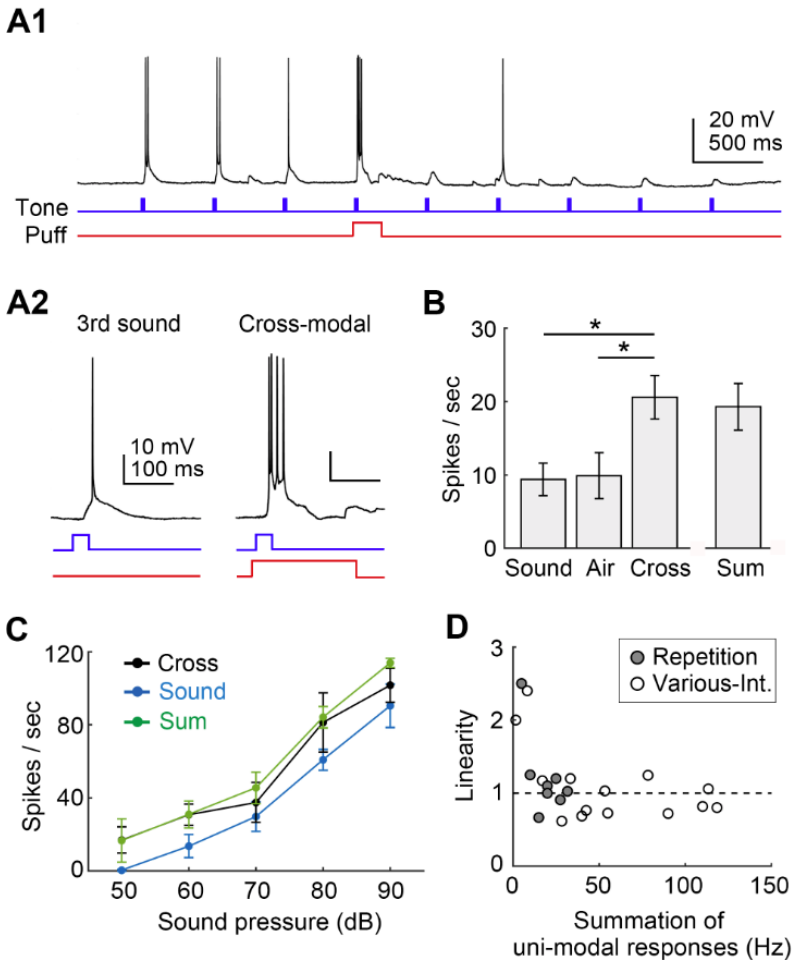

652 Figure 2-2. Multisensory enhancement of AN2 firing activity. A) Typical
653 responses to sound and cross-modal stimuli in the repetitive stimulation
654 experiments (A1), and the enlarged views of the responses to the 3rd sound
655 pulse and cross-modal stimulus combining the 4th sound pulse with airflow
656 (A2). B) Firing rates of responses to 3rd sound, airflow, and cross-modal
657 stimuli for 200 ms after stimulus onset. Cross-modal stimuli caused
658 significant increases in the firing rate than unimodal stimuli (n = 8 neurons,
659 one-way repeated measures ANOVA, $p = 0.02$; paired t-tests and Holm-
660 Bonferroni correction, cross vs. sound, $p = 0.03$; cross vs. airflow, $p =$
661 $0.09 \times 10^{-2}$; sound vs. air, $p = 0.91$). Right bar indicates the arithmetic sum
662 (Sum) of the firing responses to sound and airflow. There was no significant
663 difference in the firing rate between the sum of the unimodal responses and
664 the cross-modal responses (n = 8 neurons, paired t-test, $p = 0.39$). C) Sound
665 intensity-dependent curves of the responses to the sound (blue, n = 4 neurons),
666 cross-modal stimuli (black, n = 3 neurons excluding the point at 80 dB [n = 2
667 neurons]) and those predicted from the arithmetic sum of the unimodal
668 responses (green, n = 3 neurons). For cross-modal stimulation, the constant
669 velocity (0.17 m/s) airflow was combined with sound at various intensities (50
670 to 90 dB). D) Relationship between linearity of the cross-modal response and
671 the firing rate in summation of the unimodal responses to sound and airflow.
672 Filled circles indicate the mean value of data measured from repetitive
673 stimulation experiments for each individual (n = 8 neurons). Open circles

674 indicate the data of the response measured from various intensities of
675 stimulation experiments (n = 14 data points from 3 neurons). 'Linearity = 1'
676 shown by a dashed line indicates that the cross-modal response was equal to
677 the linear summation of the unimodal responses. 'Linearity > 1' or '< 1'
678 indicates supra- or sub-linear summation, respectively.

679 Figure 2-3

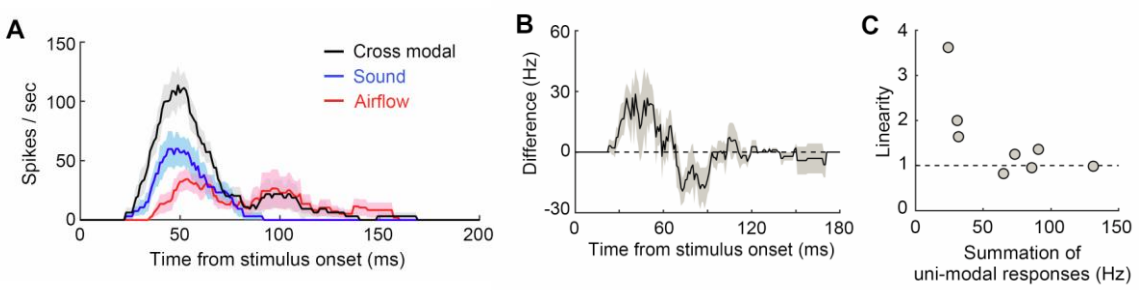


680

Figure 2-3. Dependency of linearity on latency from stimulus onset. A) Variation in the mean firing rate over time in response to cross-modal (black), sound (blue), and airflow (red) stimuli in the repetitive stimulation experiments (n = 8 neurons). B) Difference in firing rate between cross-modal responses and the summation of auditory and cercal responses (n = 8 neurons). C) Relationship between linearity of the cross-modal response and the firing rates in the summation of unimodal responses during the period of 10–60 ms after the stimulus onset, which corresponds to the period of 30–60 ms shown in F.

690 Figure 2-4

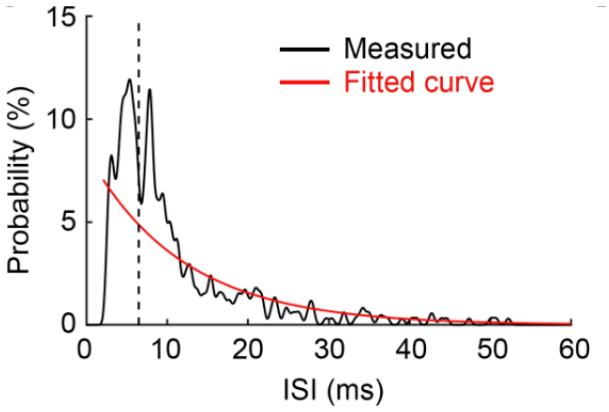

691 Figure 2-4. Distribution of ISIs measured from all spiking responses to 15-
692 kHz sound pulses of 60 dB (black; n = 424 ISIs from 16 neurons). A single
693 exponential curve was fitted to the whole distribution (red; $f(x|\mu) = \frac{1}{\mu} e^{\frac{-x}{\mu}}$,
694 $\mu = 11.87$). Dashed line indicates 6.5 ms ISI that was used for criterion of the
695 burst.

696 Figure 2-5

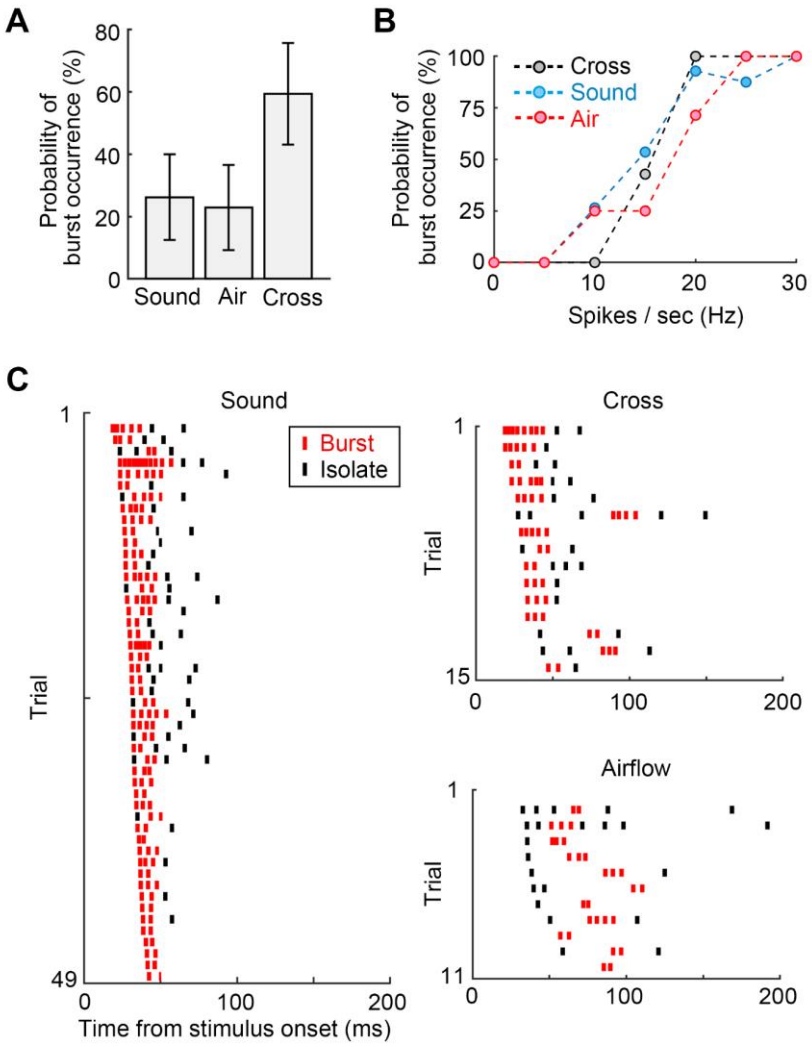

Figure 2-5. Multisensory enhancement of bursting. A) Probability of burst occurrence in the unimodal and cross-modal responses in the repetitive-stimulation experiments (n = 8 neurons, Friedman test, $p = 0.04$; Wilcoxon signed-rank test, cross vs. sound, $p = 0.13$; cross vs. air, $p = 0.06$; air vs. sound, $p = 1.00$). B) Dependency of the probability of burst generation on the firing rate in uni- and cross-modal responses. The data of both uni- and cross-modal responses were obtained from all samples in the repetitive stimulation and various intensities stimulation experiments (n = 11 neurons for sound and cross-modal) and the single airflow stimulation (n = 16 neurons for airflow). The firing rates were measured for 200 ms after the stimulus onset. C) Timing of burst firing in response to sound (left), cross-modal (upper right), and airflow (lower right) stimuli. Red and black lines indicate bursting and isolated spikes for individual trials, respectively. Each trial was sorted by the latency of the first spike. The same samples as in C were used.

711 Figure 2-6

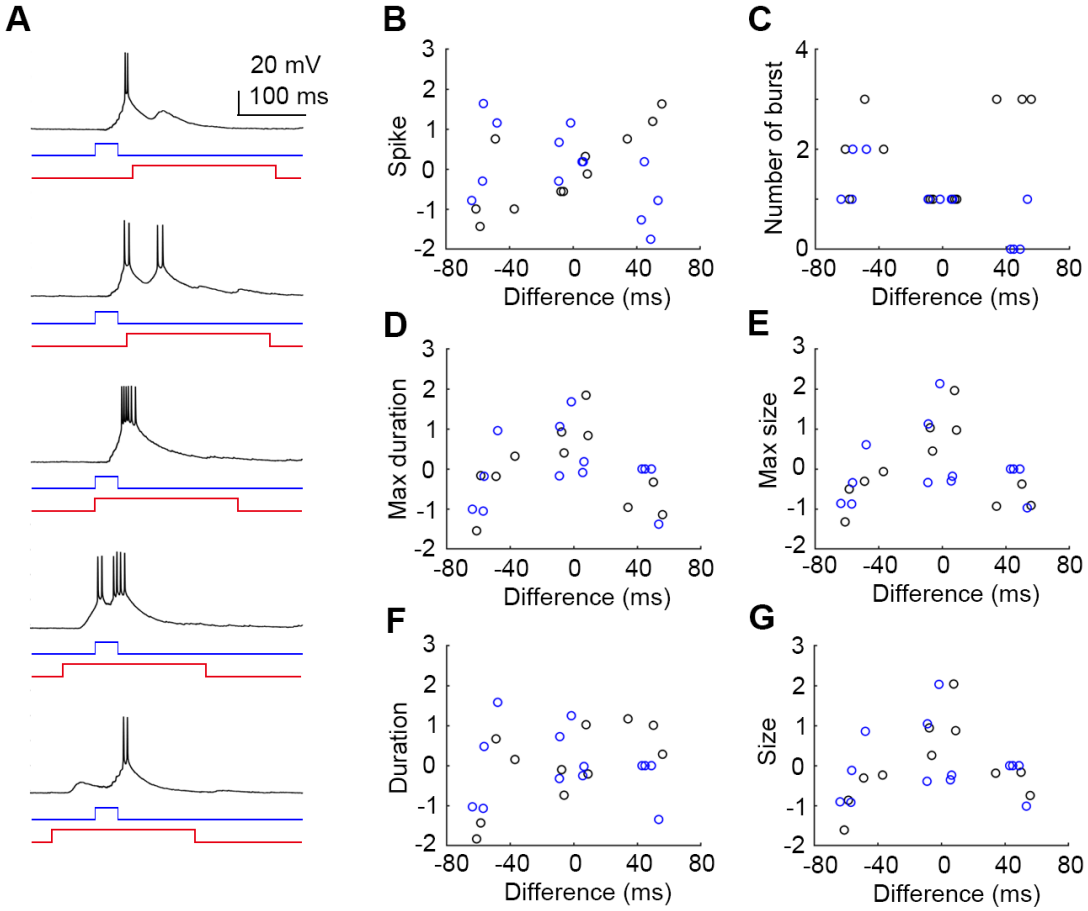


712

Figure 2-6. Dependency of the burst structures on temporal coincidence of stimulus. A) Traces of membrane potentials in AN2 in response to the combination of sound (blue) and airflow (red) stimuli with various inter-stimulus intervals. Positive value means that the onset of sound precedes the onset of airflow. B–F) Relationships between the time lag between the sound and airflow stimulus onset and firing rates normalized as Z-score (B), number of bursts (C), maximum burst duration (D), or maximum burst size (E). The values of the burst structure in (E) and (E) were measured from the largest burst in the response if multiple bursts were evoked. F, G) Summation of duration (F) and size (G) of all evoked bursts. Color indicates the data recording from different individuals through Fig. 2-6 from B to G. The max. duration and size of the burst were normalized as Z-score through D to G.

# Chapter Ⅲ

# Neural Mechanisms Underlying Multisensory Enhancement in AN2

## 3.1 Introduction

In the previous chapter, I demonstrated the effect of multisensory integration on the spiking outputs of AN2. The cross-modal stimulus combining the sound pulse and airflow enhanced spiking activities including bursting activity. And, the linearity of summation of the multisensory integration depended on the magnitude of the evoked responses. As discussed in the previous chapter, it was possible that supra-linear summation would result from the non-linear transduction from graded potentials to action potentials. To reveal the cellular mechanisms relevant to multisensory enhancement in AN2, I focused on sub-threshold changes in the membrane potential evoked by uni- and cross-modal stimuli. Also, I examined the modulation of spike threshold that affects spike outputs. In several sensory neurons, fast membrane depolarization lowers the spike threshold, which is known as a dynamic threshold (Azouz and Gray, 2003; Wilent, 2005; Jeanne and Wilson, 2015). The dynamic threshold helps neurons to detect a coincidence of inputs (Azouz and Gray, 2003; Jeanne and Wilson, 2015).

In this chapter, I investigated the difference of subthreshold activity among modalities, and between bursting and isolated spikes. And I showed the modulation of spike threshold by temporal pattern of action potentials.

## 3.2 Materials and Methods

Data, which was obtained by the experiments shown in Chapter Ⅱ, was used for the analysis. See Methods in Chapter Ⅱ about *Animals*, *Intracellular recordings* and *Stimulation*.

*Data analysis*

A burst was defined as a cluster of spikes separated by short intervals (< 6.5 ms; Marsat and Pollack, 2006). This criterion was applicable to my data as shown by figure 2-4. The first and last spike within a burst were defined as the start and end of the burst, respectively. To analyze subthreshold voltage traces, raw traces of the recordings were filtered by a median filter with a 5-ms window (Shi et al., 2017). To focus on the time variation of EPSPs, the extracted post-synaptic potentials were normalized by the potentials at the peak time of the first spike.

I adopted the following procedure to detect spike thresholds (Jeanne and Wilson, 2015). After filtering using a moving-average filter with 150-μm window, the spike threshold was defined as the membrane potential immediately preceding a spike that was detected as the inflection point in the plot of membrane potential and the slope of the potential, $dV/dt$. The inflection point was defined as the point where the $d^2V/dt^2$ fell below the 10% maximum of $d^2V/dt^2$ in the stereotypical spike trajectory. The rate of depolarization was calculated as the slope of the filtered voltage trace for 1.5

769 ms before the spike threshold. The inter-spike interval ($ISI$) of the $n^{th}$ spike
770 within a spike train was calculated from the interval between the $(n-1)^{th}$
771 and $n^{th}$ spike.

772 MATLAB software (MathWorks, RRID:SCR_001622) was used for data
773 processing and computation. All values are reported as mean ± standard error
774 of the mean. A $p$-value of $< 0.05$ was considered to be statistically significant.

## 3.3 Results

### 3.3.1 Cross-modal stimulation maintains depolarization following initial spiking

First, I compared evoked EPSPs in response to cross- and unimodal stimuli. It was technically difficult to suppress the spike generation of AN2 by injecting minus current through a sharp electrode because of cell size and geometry. Instead, the EPSPs were extracted from traces of membrane potential changes using a 5-ms median filter (Fig. 3-1A). For EPSPs evoked by airflow, the membrane potential was transiently depolarized with longer latency and decreased for 150 to 200 ms after stimulus onset even though airflow was continuously applied (Fig. 3-1B). Cross-modal stimuli evoked larger EPSPs than either unimodal stimulus types did (Fig. 3-1B), but there was no significant difference in the peak value of EPSPs among the stimulus modalities (peak potentials for cross-modal, sound, and airflow stimulation were 16.04 ± 2.11, 13.10 ± 2.28, and 12.78 ± 1.60 mV, respectively; n = 8 neurons, one-way repeated measures ANOVA, $p = 0.31$). In contrast, the EPSPs evoked by cross-modal stimuli were significantly larger in their mean during the transient elevation (0-150 ms after the stimulus onset) than those evoked by the sound and airflow stimuli (Fig. 3-1C). However, EPSP evoked by the cross-modal stimuli were much smaller in both peak and mean of potential changes than the arithmetic sum of the EPSPs evoked by sound and airflow stimuli, implying that the subthreshold potentials were sub-linearly

797 summed in AN2.

798 As shown in figure 2-5C, the cross-modal stimuli enhanced spiking
799 activity to evoke burst firing more frequently at the beginning of responses
800 compared to unimodal stimuli, suggesting differences in depolarization
801 following the first spikes in response to cross-modal versus unimodal stimuli.
802 To examine this possibility, I aligned the EPSP traces with the peak of their
803 first spikes and found that EPSPs evoked by cross-modal stimuli lasted longer
804 and had more sustained depolarization compared to EPSPs evoked by sound
805 or airflow alone (Fig. 3-2A). To quantify this, I measured the average value of
806 normalized changes in membrane potential over 6.5 ms following the first
807 spike (Fig. 3-2B). This corresponded to a border line of ISIs for separating
808 bursts and isolated spikes and probably affected the burst firing and offset of
809 the sustained peak (Fig. 3-2C), defined as the time required EPSPs to
810 decrease from 100% to 90% of the normalized potential at the first spike
811 (shown by the dashed line in Fig. 3-2A). Cross-modal stimuli evoked slightly
812 larger depolarizations after the first spike compared to unimodal stimuli, but
813 this difference was not significant (Fig. 3-2B). In contrast, the offset of peak
814 for cross-modal stimuli was significantly delayed compared to those for
815 unimodal stimuli (Fig. 3-2C). These results demonstrate that cross-modal
816 stimuli evoke longer-lasting EPSPs than unimodal stimuli.

817 The followings two factors could be considered as causes resulting in the
818 elongation of EPSP following the first spikes: the first was the time lag in the

819 response latency to the sound and airflow, the other was mechanical
820 fluctuation of the stimulus onsets of the airflow. To test the first possibility, I
821 measured the latency of the first spikes for each type of unimodal stimuli. The
822 latency of the airflow-evoked spike was significantly longer than sound- and
823 cross-modal stimulus-evoked spikes (Fig. 3-3A), meaning that the airflow
824 responses were delayed to the auditory response. From this quantification of
825 the response latencies, the time shift between the sound-evoked and airflow-
826 evoked responses was $24.10 \pm 15.81$ ms (n = 6 neurons), which was longer
827 than the offset of peak in EPSP evoked by the cross-modal stimuli ($13.88 \pm$
828 3.61 ms shown in 4F, n = 8 neurons), but no significance (Wilcoxon rank sum
829 test, $p = 0.57$). In addition, the variance of the peak offsets in the cross-modal
830 responses was much smaller than that of the time shift between the auditory-
831 and airflow-evoked first spikes (104.31 ms for the peak offset and 1500.18 ms
832 for the time lag, respectively). These facts suggest that the long-lasting peak
833 of the cross-modal responses would be partly resulted from the time difference
834 of auditory and cercal inputs, but this would not be all cause for the EPSP
835 elongation. In regard to the second possibility, I found no relationship
836 between the time lag between the sound and airflow stimulus onsets and the
837 depolarization size (Fig. 3-3B) or peak offset (Fig. 3-3C) in the EPSP evoked
838 by cross-modal stimuli, indicating that mechanical lag of the unimodal
839 stimuli had no effects on the EPSP shape.
840

### 3.3.2 Subthreshold activity accounts for burst firing in response to cross-modal stimuli in AN2.

Our results revealed differences in the time course of depolarization following the first spike in response to cross-modal and unimodal stimuli. However, it was unclear whether differences in EPSPs accounted for differences in burst firing. To investigate this hypothesis, I compared EPSPs accompanied by burst firing and by non-burst firing (isolated spikes). In responses to unimodal (sound) and cross-modal stimuli, both of which evoked bursts at the beginning of their responses (Fig. 2-5C), EPSPs accompanying bursts were larger than those accompanying isolated spikes (Fig. 3-4A1, A2). As shown in Fig. 3-2A, subthreshold potentials were normalized to the voltage at the base of the first spike and aligned with the peak time of the first spike (Fig. 3-4B1, B2), and the mean potentials over 6.5 ms following the first spike as well as the peak offset were measured. There were significant differences in mean potential changes between burst firing and isolated spikes evoked by unimodal and cross-modal stimuli (Fig. 3-4C). The peak offset for burst firing was also significantly delayed compared to that for isolated spikes in response to the unimodal and cross-modal stimuli (Fig. 3-4D). These results suggest that longer-lasting depolarization following the first spike accounted for the generation of burst firing regardless of sensory modality.

I further tested whether these parameters of the subthreshold potential are also correlated with the temporal size of bursts. Both the mean potential

863 change after the first spike and the peak offset were significantly correlated
864 with burst duration. The correlation coefficient between the peak offset and
865 the burst duration was higher (0.71) than that between the mean potential
866 change and burst duration (0.33) (Fig. 3-5A, B). However, distribution of the
867 plots for auditory and cross-modal stimuli overlapped each other. These
868 results indicated that the size and persistence of the depolarization after
869 individual spikes were key factors in determining burst generation, and that
870 the persistence of depolarization could affect the duration of the burst firing.
871 Further, both the size and persistence of EPSPs were enhanced not only by
872 multisensory integration but also by higher stimulus intensity regardless of
873 sensory modality.
874
875 **3.3.3 Inter-spike interval modulates spike threshold but modality don't.**
876 Spike output depends on the spike threshold in addition to the magnitude of
877 EPSPs. It has been reported that in some sensory systems such as Drosophila
878 olfactory neurons and mammalian visual cortical neurons, rapid membrane
879 depolarization decreases the spike threshold, creating a dynamic threshold
880 (Azouz and Gray, 2000, 2003; Jeanne and Wilson, 2015). To examine whether
881 cross-modal stimuli modulates the spike threshold in AN2, I compared spike
882 thresholds between the cross-modal and uni-modal stimulus conditions. I
883 found that the spike threshold was dynamically altered, especially during
884 burst firing (Fig. 3-6A, B); however, there was no difference in first spike

thresholds among the different stimulus modalities (Fig. 3-6C). Next, I examined which factors are related to the spike threshold. The rate of depolarization immediately preceding individual spikes was poorly correlated with the spike threshold (Fig. 3-6D). In contrast, inter-spike interval (ISI) was negatively correlated with the spike threshold regardless of the stimulation modality (Fig. 3-6E). In summary, spike threshold was dynamically altered in accordance with ISI in AN2, whereas the sensory modality had no effect on the spike threshold.

## 3.4 Discussion

I demonstrated that bimodal stimuli combining sound and airflow evoked linearly or supra-linearly summed spike outputs. In contrast, different modalities of sensory inputs were sub-linearly summed as reflected by EPSPs. Many studies on linearity in synaptic responses to cross-modal stimulation have revealed various types of computation including supra-linear, sub-linear, and linear summations. In neurons in the optic tectum of *Xenopus*, multimodal inputs are supra-linearly summed in the evoked EPSPs that result from NMDA receptor activation (Truszkowski et al., 2017). The linear summation of EPSPs is observed in the superior colliculus of rats (Skaliora et al., 2004), and sub-linear summation has been reported in the lamprey optic tectum and mouse neocortex (Olcese et al., 2013; Kardamakis et al., 2016). Thus, linearity of summation of EPSPs evoked by multimodal stimulation varies among the brain regions and animals. In previous studies, linear summation was observed as changes in membrane potential of a few millivolts from resting potentials (Skaliora et al. 2004), whereas sub-linear summation has been observed when multimodal stimuli evoke larger EPSPs close to the spike threshold (Olcese et al. 2013). In the present study, the analyzed EPSPs that were extracted from spiking responses were 'over-threshold' depolarizations by over 10 mV. Therefore, sub-linear summation in the synaptic potentials of AN2 might result from active properties of the cell membrane, which are mediated by voltage-gated cation channels.

In addition, I found the elongation of EPSP evoked by cross-modal stimuli that might result from time difference of auditory- and cercal-sensory inputs. AN2 receives direct excitatory inputs from the auditory receptor afferents (Hennig 1988) whereas cercal sensory inputs are mediated by at least 2 synapses that include synapses from mechanoreceptor afferents to cercal projection neurons such as GIs and that from those projection neurons to AN2. It is possible that the cercal sensory pathway may involve in other prothoracic interneurons. AN2 might apply the time difference of multisensory inputs to elongate the compound EPSP generating the burst firings.

The modulation of spike threshold has been observed in some sensory neurons (Azouz and Gray, 2003; Wilent, 2005). In these neurons, the rate of depolarization modulates the spike threshold. In AN2, the rate of depolarization and sensory modality did not affect the spike threshold whereas the spike threshold was modulated by the inter-spike interval. This intrinsic property might prevent the generation of inappropriate bursts.

932 Figure 3-1

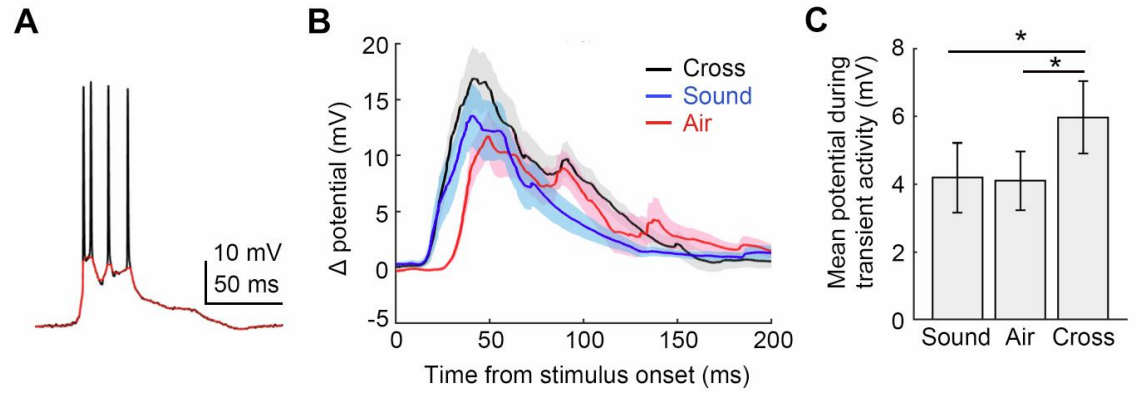

933 Figure 3-1. Excitatory post-synaptic potentials (EPSPs) evoked by cross-
934 modal and unimodal stimuli. A) Extracted PSPs. Action potentials were
935 removed from the raw trace of membrane potential (black trace) using a 5-ms
936 median filter to estimate the graded potential of PSPs (red trace). B) Time
937 variation in the membrane potential changes in EPSPs evoked by cross-modal
938 (black), sound (blue), and airflow (red) stimuli in repetitive stimulation
939 experiments (n = 8 neurons). C) Mean changes of membrane potential in
940 EPSPs for 150 ms after the stimulus onset (n = 8 neurons, Friedman test,
941 $p = 0.01$; Wilcoxon signed-rank test with Holm-Bonferroni correction, cross vs.
942 sound, $p = 0.47 \times 10^{-1}$; cross vs. air, $p = 0.02$; sound vs. air, $p = 0.84$).

943 Figure 3-2

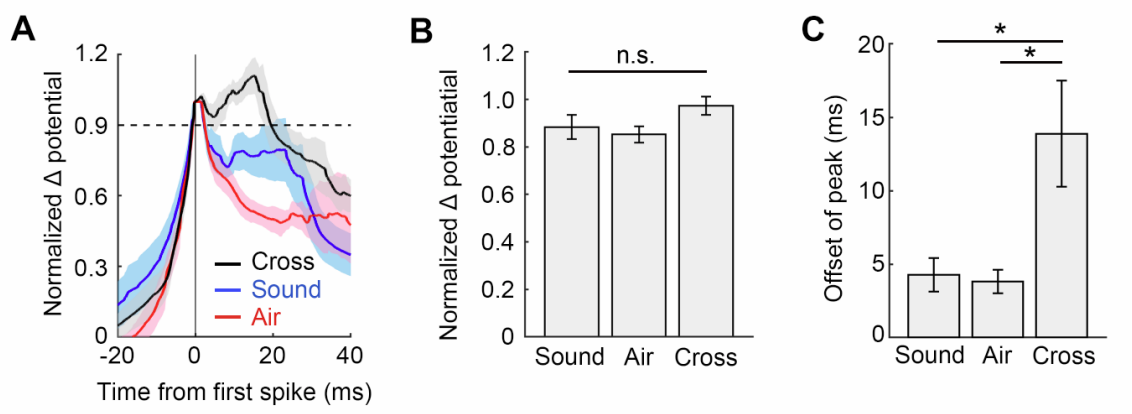

944 Figure 3-2. EPSPs relevant to first spike for stimulus. A) Time variation in
945 graded potential changes in EPSPs following the first spike. EPSP traces
946 were temporally aligned to peak time of the first spike and normalized in
947 magnitude by a value of the graded potentials at that moment (n = 8, 7, and
948 7 neurons for cross-modal, sound, and airflow, respectively). The dashed line
949 indicates 90% of the EPSP at the time of the first spike (0 ms). E, F) Mean
950 values of the normalized changes in membrane potential over 6.5 ms
951 following the first spike (E; n = 8, 7, and 7 neurons for cross-modal, sound,
952 and airflow, respectively. Kruskal-Wallis test, $p = 0.14$) and the offset of peak
953 EPSPs (F; n = 8, 7, and 7 neurons for cross-modal, sound, and airflow,
954 respectively, One-way factorial ANOVA, $p = 0.01$; unpaired t-test with Holm-
955 Bonferroni correction, cross vs. sound, $p = 0.02$; cross vs. air, $p = 0.02$; sound
956 vs. air, $p = 0.47$) evoked by different modalities of stimuli. The offset of peak
957 was measured as the time when EPSPs were > 90% of the normalized EPSP
958 indicated by the broken line in D.

959 Figure 3-3.

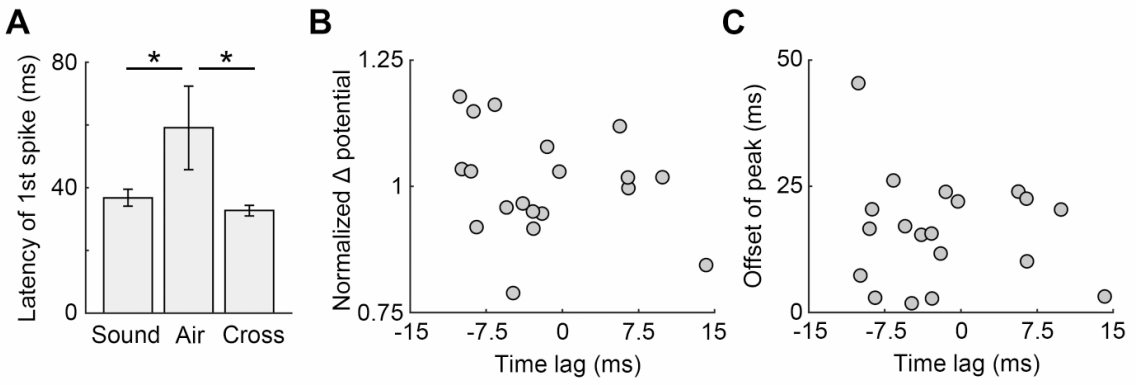

960 Figure 3-3. Effects of the time difference in response latency and in stimulus
961 onset on EPSP's properties. A) Latency of the first spikes evoked by different
962 types of stimulation from the stimulus onset. The spike latency of the airflow
963 response was significantly longer than those of sound and cross-modal
964 responses (n = 7, 7, and 8 neurons for sound, airflow and cross-modal
965 stimulations, respectively, Kruskal-Wallis test, $p = 0.04 \times 10^{-1}$; Wilcoxon
966 rank sum test with Holm-Bonferroni correction, sound vs. air, $p = 0.04$; cross
967 vs. air, $p = 0.04 \times 10^{-1}$; sound vs. cross, $p = 0.28$). B, C) Relationships
968 between the time lag between the sound and airflow stimulus onset and the
969 normalize membrane potentials within 6.5 ms after the 1st spike peak (B) or
970 the offset of peak (C) in EPSPs evoked by cross-modal stimuli (n = 19
971 responses from 8 neurons, Spearman's rank correlations, $r = -0.32$, $p = 0.18$
972 for B, $r = -0.04$, $p = 0.89$ for C). Negative value of the time lag indicates
973 that the airflow preceded the combined sound stimulus onset.

974 Figure 3-4

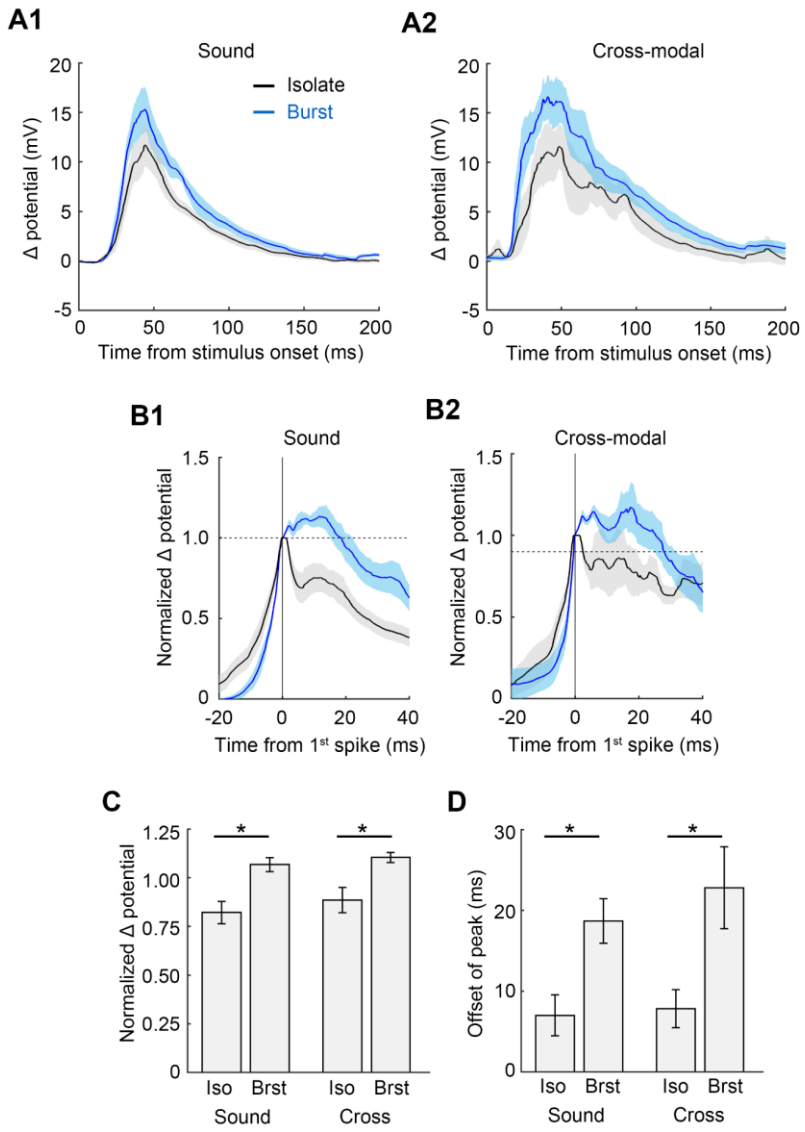

975 Figure 3-4. Excitatory post-synaptic potential (EPSP) characteristics
976 affecting burst firing. A) Extracted EPSPs accompanied by isolated spikes
977 (black) or burst firing (blue) in response to sound (A1) and cross-modal (A2)
978 stimuli. All data used for Figure 3-4 were obtained from the responses to uni-
979 and cross-modal stimuli using 60-dB sound in both the repetitive stimulation
980 and various intensities of stimulation experiments. Sample sizes used for A
981 to D were n = 8 and 5 neurons for isolated spikes and bursts evoked by sound
982 stimuli, and n = 9 and 7 neurons for isolated spikes and bursts evoked by
983 cross-modal stimulation, respectively. B) Time variation of the graded
984 potential changes in EPSPs following the first spike evoked by sound (B1) or
985 cross-modal (B2) stimuli. Colors of lines correspond to those in A. C, D) Mean
986 values of the normalized changes in membrane potential for 6.5 ms after the
987 first spike (C; Wilcoxon rank sum test, isolated vs. burst for sound stimuli,
988 $p = 0.03 \times 10^{-1}$; isolated vs. burst for cross-modal stimuli, $p = 0.05 \times 10^{-1}$)
989 and of the offset of peak in EPSPs (D; unpaired t-test, isolated vs. burst for
990 sound stimuli, $p = 0.01$; isolated vs. burst for cross-modal stimuli, $p = 0.01$)
991 accompanied by isolated spikes or bursts in response to sound and cross-
992 modal stimuli.
993

994 Figure 3-5

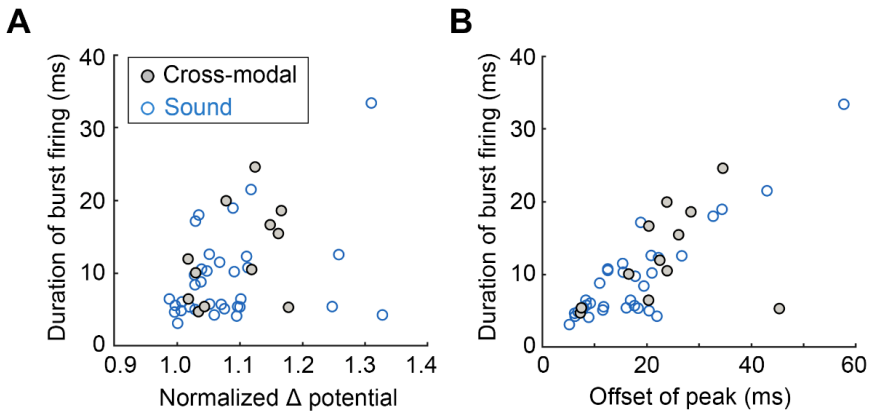

995 Figure 3-5. EPSP characteristics relevant to structure of burst. A, B)
996 Relationship between the duration of burst firing and the mean of normalized
997 potential changes (A; n = 46 burst responses from 10 neurons, Spearman's
998 rank correlation, $r = 0.33$, $p = 0.02$) or the offset of peak EPSPs (B; sample
999 size was the same as in A, Spearman's rank correlation, $r = 0.71$; $p =$
1000 $0.03 \times 10^{-6}$). Blue open circles represent data for sound stimuli and gray filled
1001 circles represent data for cross-modal stimuli.

1002 Figure 3-6

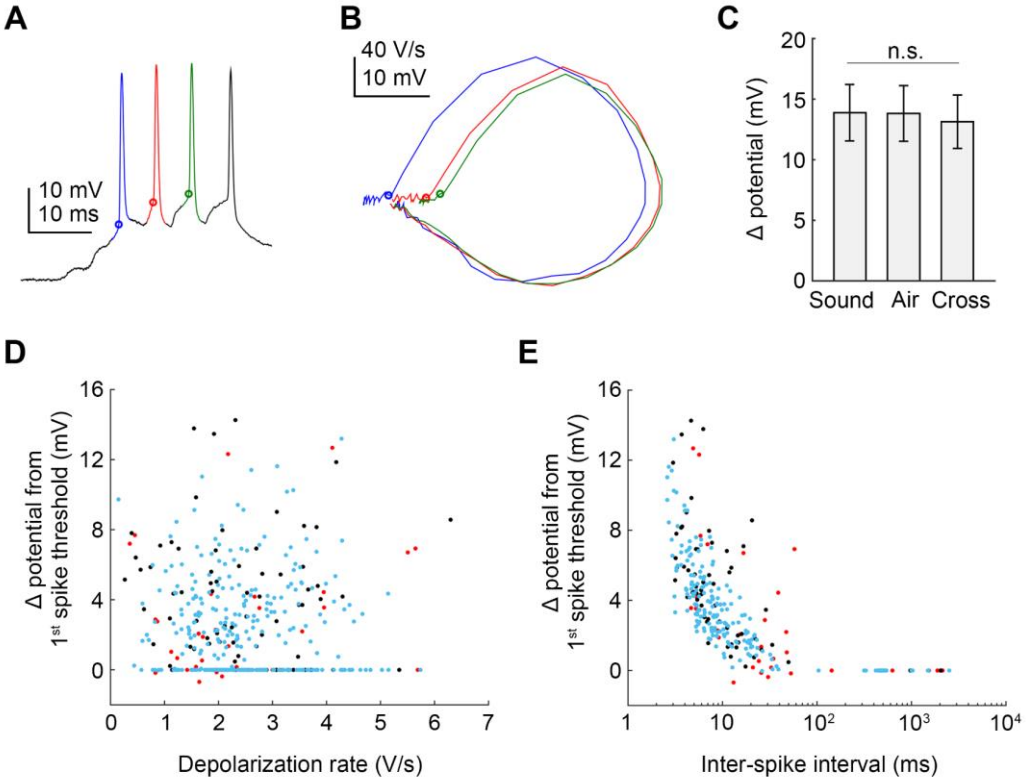

Figure 3-6. Modulation of the spike threshold in AN2. A) Trace of a typical firing response and estimated spike threshold potentials. Blue, red, and green circles indicate the threshold for the first, second, and third spikes, respectively. B) Phase portraits ($dV/dt$ versus $V$) for the 3 spikes shown in A. Colors of traces correspond to those in A. C) Thresholds of the first spikes evoked by different modalities of stimuli (n = 7, 7 and 8 neurons; One-way factorial ANOVA, $p = 0.81$). Delta potentials of spike thresholds were the differences between the threshold potential and resting membrane potential before stimuli. D, E) Relationship between spike threshold and the preceding depolarization rate (D; Spearman's rank correlation, $r_{cross} = -0.20$, $r_{sound} = -0.07$, and $r_{airflow} = 0.05$; $p_{cross} = 0.08$, $p_{sound} = 0.22$, and $p_{airflow} = 0.73$) or inter-spike interval (E; Spearman's rank correlation, $r_{cross} = -0.84$, $r_{sound} = -0.92$, and $r_{airflow} = -0.68$; $p_{cross} = 1.59 \times 10^{-21}$, $p_{sound} = 1.98 \times 10^{-119}$, and $p_{airflow} = 4.00 \times 10^{-7}$). Sample size shown in D was the same as shown in E (n = 293, 44 and 78 spike thresholds from 8, 7 and 8 neurons in sound, air and cross-modal stimulations respectively). The depolarization rate was measured as the slope of the change in membrane potential for 1.5 ms prior to each spike-threshold point. Delta (Δ) potential from first spike threshold was measured as the difference between the threshold potential and the first spike threshold. Colors of dots in D and E indicate data for cross-modal (black), sound (blue), and airflow (red) stimuli.

## General Discussion

Multisensory integration is fundamental computation observed in various sensory systems and different brain regions (Meredith and Stein, 1986; Ghazanfar and Schroeder, 2006; Deeg et al., 2009; Zahar et al., 2009; Kardamakis et al., 2016). Multisensory integration is performed in not only higher processing stage for association but also earlier stages close to sensory surface such as the primary auditory cortex of macaque and the primary visual cortex of mouse (Schroeder and Foxe, 2005; Ghazanfar and Chandrasekaran, 2007; Lakatos et al., 2007; Ibrahim et al., 2016). In Drosophila larvae, certain sensory neurons directly receive sensory inputs from receptor cells of different modalities (Ohyama et al., 2015). The prothoracic auditory circuit of crickets is also such a sensory system to integrate various modalities in the early stage as discussed in Chapter I. These findings imply that multisensory integration is fundamental mechanisms in early stage of sensory processing.

Finally, I refer to the behavioral relevance of multisensory integration in AN2. AN2 is considered to play a crucial role in the detection of predatory bats, because it is sensitive to ultrasound-like echolocation calls of bats, and its firing activity is necessary and sufficient to trigger avoidance steering in the opposite direction of the sound source (Nolen and Hoy, 1984, 1986). Notably, bursting of AN2 correlates with abdominal movement in the avoidance steering behavior (Marsat and Pollack 2006, 2010). I demonstrated

1047 that AN2 generates bursting in response to 15-kHz tone pulses of which the
1048 carrier frequency was lower than that used in previous studies (Marsat and
1049 Pollack 2006, 2007, 2010), and that cross-modal stimuli combining the tone
1050 pulse with airflow enhanced the generation of bursting. AN2 represents
1051 directionality, intensity, and duration of sound stimuli with its bursting
1052 (Marsat and Pollack, 2006, 2010). Our results, therefore, suggest that
1053 multisensory integration in AN2 may enable quicker and more precise
1054 identification of alert signals via simultaneous detection of the searching echo
1055 and air flow caused by flying bats.

1056 The avoidance steering driven by the bursts of the AN2 are observed
1057 only in response to ultrasound during flight. So, it remains unclear whether
1058 flying crickets use wind stimuli as a sign of a bat's attack. Several types of
1059 insects, such as mantids and cockroaches, detect the predator's attack by
1060 their cercal organs and execute avoidance steering during flight (Ganihar et
1061 al., 1994; Triblehorn and Yager, 2006). It is possible that the wind sensitivity
1062 of AN2 might be useful for successful escape via multisensory integration
1063 with auditory inputs. On the other hand, crickets standing on the ground
1064 exhibit escape behaviors such as running or jumping in response to wind
1065 stimuli (Tauber and Camhi, 1995; Oe and Ogawa, 2013; Sato et al., 2017).
1066 AN2 is also involved in the phonotaxis via detection of conspecific calls
1067 (Schildberger and Hörner, 1988), meaning that AN2 could respond to
1068 ultrasound and also to airflow in standing crickets. Recently, I reported that

10- or 15-kHz pure tones that will activate AN2 modulate wind-elicited escape behavior in crickets (Fukutomi et al., 2015; Fukutomi and Ogawa, 2017). Taken together, the findings in this study suggest that AN2 is an excellent model for understanding the neuroethological significance of multisensory integration.

1074 **Reference**

1075 Alais D, Burr D (2004) The ventriloquist effect results from near-optimal
1076 bimodal integration. Curr Biol 14:257–262.
1077 Atilgan H, Town SM, Wood KC, Jones GP, Maddox RK, Lee AKC, Bizley JK
1078 (2018) Integration of visual information in auditory cortex promotes
1079 auditory scene analysis through multisensory binding. Neuron 97:640–
1080 655.
1081 Atkins G, Pollack GS (1987) Response properties of prothoracic,
1082 interganglionic, sound-activated interneurons in the cricketTeleogryllus
1083 oceanicus. J Comp Physiol A 161:681–693.
1084 Azouz R, Gray CM (2000) Dynamic spike threshold reveals a mechanism for
1085 synaptic coincidence detection in cortical neurons in vivo. Proc Natl Acad
1086 Sci 97:8110–8115.
1087 Azouz R, Gray CM (2003) Adaptive coincidence detection and dynamic gain
1088 control in visual cortical neurons in vivo. Neuron 37:513–523.
1089 Bastian J, Nguyenkim J (2001) Dendritic modulation of burst-like firing in
1090 sensory neurons. J Neurophysiol 85:10–22.
1091 Deeg KE, Sears IB, Aizenman CD (2009) Development of multisensory
1092 convergence in the xenopus optic tectum. J Neurophysiol 102:3392–3404.
1093 Ernst MO, Banks MS (2002) Humans integrate visual and haptic information
1094 in a statistically optimal fashion. Nature 415:429.
1095 Fetsch CR, DeAngelis GC, Angelaki DE (2013) Bridging the gap between

1096 theories of sensory cue integration and the physiology of multisensory
1097 neurons. Nat Rev Neurosci 14:429–442.
1098 Fotowat H, Gabbiani F (2007) Relationship between the phases of sensory
1099 and motor activity during a looming-evoked multistage escape behavior.
1100 J Neurosci 27:10047–10059.
1101 Fukutomi M, Ogawa H (2017) Crickets alter wind-elicited escape strategies
1102 depending on acoustic context. Sci Rep 7:15158.
1103 Fukutomi M, Someya M, Ogawa H (2015) Auditory modulation of wind-
1104 elicited walking behavior in the cricket Gryllus bimaculatus. J Exp Biol
1105 218:3968–3977.
1106 Ganihar D, Libersat F, Wendler G, Camhi JM (1994) Wind-evoked evasive
1107 responses in flying cockroaches. J Comp Physiol A 175:49–65.
1108 Ghazanfar AA, Chandrasekaran CF (2007) Paving the way forward:
1109 integrating the senses through phase-resetting of cortical oscillations.
1110 Neuron 53:162–164.
1111 Ghazanfar A, Schroeder C (2006) Is neocortex essentially multisensory?
1112 Trends Cogn Sci 10:278–285.
1113 Gu Y, Angelaki DE, DeAngelis GC (2008) Neural correlates of multisensory
1114 cue integration in macaque MSTd. Nat Neurosci 11:1201–1210.
1115 Hennig RM (1988) Ascending auditory interneurons in the
1116 cricketTeleogryllus commodus (Walker): comparative physiology and
1117 direct connections with afferents. J Comp Physiol A 163:135–143.

1118 Herberholz J, Marquart G (2012) Decision making and behavioral choice
1119 during predator avoidance. Front Neurosci 6:125.
1120 Hirota K, Yuji S, Yoshichika B, Tsuneo Y, others (1993) Distinction in
1121 morphology and behavioral role between dorsal and ventral groups of
1122 cricket giant interneurons. Zoolog Sci 10:705–709.
1123 Holmes NP, Spence C (2005) Multisensory Integration: Space, time and
1124 superadditivity. Curr Biol 15:762–764.
1125 Horseman G, Huber F (1994) Sound localisation in crickets. J Comp Physiol
1126 A 175:389–398.
1127 Hoy R, Nolen T, Brodfuehrer P (1989) The neuroethology of acoustic startle
1128 and escape in flying insects. J Exp Biol 146:287–306.
1129 Ibrahim LA, Mesik L, Ji X, Fang Q, Li H, Li Y, Zingg B, Zhang LI, Tao HW
1130 (2016) Cross-modality sharpening of visual cortical processing through
1131 layer-1-mediated inhibition and disinhibition. Neuron 89:1031–1045.
1132 Imaizumi K, Pollack GS (1999) Neural coding of sound frequency by cricket
1133 auditory receptors. J Neurosci 19:1508–1516.
1134 Imaizumi K, Pollack GS (2005) Central projections of auditory receptor
1135 neurons of crickets. J Comp Neurol 493:439–447.
1136 Jacobs GA, Miller JP, Aldworth Z (2008) Computational mechanisms of
1137 mechanosensory processing in the cricket. J Exp Biol 211:1819–1828.
1138 Jeanne JM, Wilson RI (2015) Convergence, divergence, and reconvergence in
1139 a feedforward network improves neural speed and accuracy. Neuron

88:1014–1026.

Kardamakis AA, Pérez-Fernández J, Grillner S (2016) Spatiotemporal interplay between multisensory excitation and recruited inhibition in the lamprey optic tectum. Elife 5:e16472.

Kidokoro-Kobayashi M, Iwakura M, Fujiwara-Tsujii N, Fujiwara S, Sakura M, Sakamoto H, Higashi S, Hefetz A, Ozaki M (2012) Chemical discrimination and aggressiveness via cuticular hydrocarbons in a supercolony-forming ant, Formica yessensis. PLoS One 7:e46840.

Klapoetke NC, Nern A, Peek MY, Rogers EM, Breads P, Rubin GM, Reiser MB, Card GM (2017) Ultra-selective looming detection from radial motion opponency. Nature 551:237.

Kühne R, Silver S, Lewis B (1984) Processing of vibratory and acoustic signals by ventral cord neurones in the cricket Gryllus campestris. J Insect Physiol 30:575–585.

Lakatos P, Chen C-M, O'Connell MN, Mills A, Schroeder CE (2007) Neuronal oscillations and multisensory interaction in primary auditory cortex. Neuron 53:279–292.

Marsat G, Pollack GS (2005) Effect of the temporal pattern of contralateral inhibition on sound localization cues. J Neurosci 25:6137–6144.

Marsat G, Pollack GS (2006) A behavioral role for feature detection by sensory bursts. J Neurosci 26:10542–10547.

Marsat G, Pollack GS (2007) Efficient inhibition of bursts by bursts in the

auditory system of crickets. J Comp Physiol A 193:625–633.

Marsat G, Pollack GS (2010) The structure and size of sensory bursts encode stimulus information but only size affects behavior. J Comp Physiol A 196:315–320.

Marsat G, Pollack GS (2012) Bursting neurons and ultrasound avoidance in crickets. Front Neurosci 6:95.

McMeniman CJ, Corfas RA, Matthews BJ, Ritchie SA, Vosshall LB (2014) Multimodal integration of carbon dioxide and other sensory cues drives mosquito attraction to humans. Cell 156:1060–1071.

Meredith MA, Stein BE (1986) Visual, auditory, and somatosensory convergence on cells in superior colliculus results in multisensory integration. J Neurophysiol 56:640–662.

Meredith M, Stein B (1983) Interactions among converging sensory inputs in the superior colliculus. Science 221:389–391.

Miller JP, Jacobs GA, Theunissen FE (1991) Representation of sensory information in the cricket cercal sensory system. I. Response properties of the primary interneurons. J Neurophysiol 66:1680–1689.

Miller JP, Krueger S, Heys JJ, Gedeon T (2011) Quantitative characterization of the filiform mechanosensory hair array on the cricket cercus. PLoS One 6:e27873.

Nolen TG, Hoy RR (1984) Initiation of behavior by single neurons: the role of behavioral context. Science 226:992–994.

1184 Nolen TG, Hoy RR (1986) Phonotaxis in flying crickets. I. Attraction to the
1185 calling song and avoidance of bat-like ultrasound are discrete behaviors.
1186 J Comp Physiol A 159:423–439.
1187 Oe M, Ogawa H (2013) Neural basis of stimulus-angle-dependent motor
1188 control of wind-elicited walking behavior in the cricket Gryllus
1189 bimaculatus. PLoS One 8:e80184.
1190 Ohyama T, Schneider-Mizell CM, Fetter RD, Aleman JV, Franconville R,
1191 Rivera-Alba M, Mensh BD, Branson KM, Simpson JH, Truman JW,
1192 Cardona A, Zlatic M (2015) A multilevel multimodal circuit enhances
1193 action selection in Drosophila. Nature 520:633.
1194 Olcese U, Iurilli G, Medini P (2013) Cellular and synaptic architecture of
1195 multisensory integration in the mouse neocortex. Neuron 79:579–593.
1196 Palka J, Olberg R (1977) The cercus-to-giant interneuron system of crickets.
1197 J Comp Physiol 119:301–317.
1198 Perrault TJ, Vaughan JW, Stein BE, Wallace MT (2003) Neuron-specific
1199 response characteristics predict the magnitude of multisensory
1200 integration. J Neurophysiol 90:4022–4026.
1201 Perrault TJ, Vaughan JW, Stein BE, Wallace MT (2005) Superior colliculus
1202 neurons use distinct operational modes in the integration of multisensory
1203 stimuli. J Neurophysiol 93:2575–2586.
1204 Pollack GS (2015) Neurobiology of acoustically mediated predator detection.
1205 J Comp Physiol A 201:99–109.

Popov AV, Markovich AM (1982) Auditory interneurones in the prothoracic ganglion of the cricket,Gryllus bimaculatus. J Comp Physiol A 146:351–359.

Pouget A, Deneve S, Duhamel JR (2002) A computational perspective on the neural basis of multisensory spatial representations. Nat Rev Neurosci 3:741–747.

Rowland BA, Quessy S, Stanford TR, Stein BE (2007) Multisensory integration shortens physiological response latencies. J Neurosci 27:5879–5884.

Rowland B, Stein B (2007) Multisensory integration produces an initial response enhancement. Front Integr Neurosci 1:4.

Sato N, Shidara H, Ogawa H (2017) Post-molting development of wind-elicited escape behavior in the cricket. J Insect Physiol 103:36–46.

Schildberger K, Hörner M (1988) The function of auditory neurons in cricket phonotaxis. J Comp Physiol A 163:621–631.

Schroeder CE, Foxe J (2005) Multisensory contributions to low-level, "unisensory" processing. Curr Opin Neurobiol 15:454–458.

Selverston AI, Kleindienst HU, Huber F (1985) Synaptic connectivity between cricket auditory interneurons as studied by selective photoinactivation. J Neurosci 5:1283–1292.

Shi X, Barchini J, Ledesma HA, Koren D, Jin Y, Liu X, Wei W, Cang J (2017) Retinal origin of direction selectivity in the superior colliculus. Nat

1228 Neurosci 20:550–558.
1229 Skaliora I, Doubell TP, Holmes NP, Nodal FR, King AJ (2004) Functional
1230 topography of converging visual and auditory inputs to neurons in the
1231 rat superior colliculus. J Neurophysiol 92:2933–2946.
1232 Stanford TR (2005) Evaluating the operations underlying multisensory
1233 integration in the cat superior colliculus. J Neurosci 25:6499–6508.
1234 Stein BE, Scott Huneycutt W, Alex Meredith M (1988) Neurons and behavior:
1235 the same rules of multisensory integration apply. Brain Res 448:355–358.
1236 Stein BE, Stanford TR (2008) Multisensory integration: current issues from
1237 the perspective of the single neuron. Nat Rev Neurosci 9:255–266.
1238 Tauber E, Camhi J (1995) The wind-evoked escape behavior of the cricket
1239 Gryllus bimaculatus: integration of behavioral elements. J Exp Biol
1240 198:1895–1907.
1241 Theunissen FE, Miller JP (1991) Representation of sensory information in
1242 the cricket cercal sensory system. II. Information theoretic calculation of
1243 system accuracy and optimal tuning-curve widths of four primary
1244 interneurons. J Neurophysiol 66:1690–1703.
1245 Triblehorn JD, Yager DD (2006) Wind generated by an attacking bat:
1246 anemometric measurements and detection by the praying mantis cercal
1247 system. J Exp Biol 209:1430–1440.
1248 Truszkowski TLS, Carrillo OA, Bleier J, Ramirez-Vizcarrondo CM, Felch DL,
1249 McQuillan M, Truszkowski CP, Khakhalin AS, Aizenman CD (2017) A

cellular mechanism for inverse effectiveness in multisensory integration. Elife 6:e25392.

Wiese K (1981) Influence of vibration on cricket hearing: Interaction of low frequency vibration and acoustic stimuli in the omega neuron. J Comp Physiol A 143:135–142.

Wilent WB (2005) Stimulus-dependent changes in spike threshold enhance feature selectivity in rat barrel cortex neurons. J Neurosci 25:2983–2991.

Wohlers DW, Huber F (1978) Intracellular recording and staining of cricket auditory interneurons (Gryllus campestris L.,Gryllus bimaculatus DeGeer). J Comp Physiol A 127:11–28.

Wohlers DW, Huber F (1982) Processing of sound signals by six types of neurons in the prothoracic ganglion of the cricket,Gryllus campestris L. J Comp Physiol 146:161–173.

Zahar Y, Reches A, Gutfreund Y (2009) Multisensory enhancement in the optic tectum of the barn owl: Spike count and spike timing. J Neurophysiol 101:2380–2394.

## Acknowledgment

First of all, I would like to express my sincere gratitude to Professor Hiroto Ogawa, me supervisor for giving me a great support, insightful comments. I learned not only electrophysiological techniques but also how to justly approach scientific questions.

I am also most grateful to Dr. Hokto Kazama (Riken Brain Science Institute), Professor Makoto Mizunami and Professor Toshiya Mastushima for giving me critical comments and suggestions as members of dissertation committee. I appreciate Dr. Hokto Kazama for giving me an opportunity to discuss about my study with researchers working in Riken Brain Science Institute. I thank Dr. Berthold Hedwig for providing the techniques of intracellular recording in the cricket's auditory system.

I also appreciate the financial support of Japan Society for Promotion of Science, Grant-in-Aid for JSPS Research Fellow 15J02077.

**Publication**

Makoto Someya and Hiroto Ogawa:

"Multisensory enhancement of burst activity in an insect auditory neuron"

*Journal of Neurophysiology,* doi: 10.1152/jn.00798.2017.

**Presentation:**

[International]

Someya M, Ogawa H (2017) Coincident multisensory inputs enhance burst activity via large and long-lasting EPSPs in insect auditory neuron, poster, Society for Neuroscience 47th Annual Meeting, Washington, DC, USA.

Someya M, Ogawa H (2014) Multisensory integration of auditory and cercal sensory inputs by ascending projection neurons in the cricket, poster, The 11th International Congress of Neuroethology, Sapporo, Japan.

[Domestic]

Someya M, Ogawa H (2017) Multisensory integration of auditory and mechanosensory inputs in identified projection neuron in the cricket, oral, The 40th Annual Meeting of the Japan Neuroscience Society, Yokohama, Japan.

Someya M, Ogawa H (2016) Multisensory integration in early stage of sensory processing of cricket, poster, The 39th Annual Meeting of the Japan Neuroscience Society, Yokohama, Japan.

1303 Someya M, Ogawa H (2014) Multisensory ascending neurons responding to
1304 auditory and airflow stimuli in the cricket, poster, The 37th Annual Meeting
1305 of the Japan Neuroscience Society, Yokohama, Japan.
1306 Someya M, Ogawa H. (2013) Neural representation of directional information
1307 in different sensory modalities, poster, The 36th Annual Meeting of the Japan
1308 Neuroscience Society, Kyoto, Japan.